IMPLEMENTATION AND VALIDATION OF AN UNSTRUCTURED COUPLED WAVE-CIRCULATION MODEL FOR HURRICANE WAVE AND STORM SURGE INUNDATION MODELING IN PUERTO RICO

by

Juan Orlando González López

A thesis submitted in partial fulfillment of the requirements for the degree of

MASTER OF SCIENCE
in
MARINE SCIENCES
PHYSICAL OCEANOGRAPHY

UNIVERSITY OF PUERTO RICO
MAYAGÜEZ CAMPUS
2010

Approved by:

_____	_____
Aurelio Mercado, MS President, Graduate Committee	Date
_____	_____
Julio Morell, MS Member, Graduate Committee	Date
_____	_____
Jorge Capella, Ph.D. Member, Graduate Committee	Date
_____	_____
Basir Shafiq, Ph.D. Representative of Graduate Studies	Date
_____	_____
Nilda Aponte, Ph.D. Department of Marine Sciences Chair	Date

Abstract

An unstructured wave-circulation coupled model is implemented and validated for Puerto Rico. The model is used to simulate Hurricane Georges and Hurricane Omar to validate the hurricane-forced storm surge water levels and wave fields. Two parametric wind field formulations are used to produce the wind fields and evaluate the effects of each formulation on wave and water level results. To explore the effect of mesh resolution on wave-induced forces and storm surge water levels a comparison is done between the results of the unstructured coupled model and a simulation using the circulation model coupled to a high resolution (30 meters) structured wave model in the area of La Parguera. Results show a good agreement between the observed and the modeled water levels. The steep and complex bathymetry demands that the unstructured mesh is further optimized to properly resolve the wave and circulation processes at the finer near shore scale.

Resumen

Un modelo acoplado no-estructurado de olaje y circulación es implementado y validado para Puerto Rico. El modelo se utiliza para simular el Huracán Georges y el Huracán Omar para validar la marejada ciclónica y el oleaje forzado por huracanes. Dos formulaciones paramétricas se utilizan para simular el campo de vientos y evaluar sus efectos en la marejada ciclónica y el oleaje resultante. Para explorar el efecto de la resolución de la malla en las fuerzas inducidas por oleaje y la marejada ciclónica se comparan el modelo acoplado no-estructurado y un acoplamiento con un modelo estructurado de olas a una alta resolución de 30 metros en el área de La Parguera. Los resultados demuestran un buen acuerdo entre la marejada ciclónica observada y la simulada. La batimetría abrupta y compleja de la región exige que la malla no-estructurada sea optimizada para resolver apropiadamente los procesos de oleaje y circulación a pequeña escala en la costa.

A mis padres que me han enseñado la importancia de la educación.

Acknowledgements

First and foremost to my graduate committee who guided me through these years and introduced me to the world of oceanography and fluid dynamics, along with Dr. Jorge Corredor, Dr. Jose Lopez, and Dr. Miguel Canals. To the Caribbean Integrated Coastal Ocean Observing System (CarICOOS) and the Department of Environmental and Natural Resources Coastal Zone Management Program who provided the funding for this study. Dr. Joannes Westerink and Dr. Casey Dietrich from the Computational Hydraulics Lab at University of Notre Dame, who developed the ADCIRC+unSWAN model and were eager to discuss ideas and results; and Dr. Brian Blanton at University of North Carolina – Chapel Hill who initially taught me how to run and set up the ADCIRC model.

Table of Contents

List of Tables

List of Figures

1 Introduction

Puerto Rico has a diverse coastal geomorphology that ranges from a narrow shelf at the north and southeastern coast to a wider shelf with numerous fringing reefs at the southwestern coast. The wave regime differs greatly at each coast due to the influence of the Atlantic Ocean at the north and the Caribbean Sea at the south coast, as well as the difference between the wave transformation processes that occur in narrow versus wider, reef-featured shelves (Morelock 1978). Such a great variation in bathymetric features and dynamic ocean processes demand that numerical models capable of solving the dynamics at such varied scales be used.

The ADCIRC+unSWAN (Dietrich, et al. 2010) model couples both a finite-element shallow-water circulation model and a wind-wave spectral model into an unstructured mesh capable of representing variable spatial resolution ranging from the order of meters to kilometers in the same mesh. In this way both circulation and wave processes that lead to storm surge and coastal inundation can be solved at basin and coastal scales, with higher resolution at areas where complex bathymetry steers the ocean dynamics and coarser resolution where the bathymetry does not results in complex flows or wave fields. This leads to computational efficiency as higher resolution is directed towards areas where complex processes need to be solved while at the same time relaxing resolution at other areas in the same mesh, eliminating the need for regular mesh nesting and interpolation between different computational grids for circulation and wave models.

In this thesis the ADCIRC+unSWAN model is implemented and validated for Puerto Rico. The model is used to simulate Hurricane Georges and Hurricane Omar to validate the hurricane-forced storm surge water levels and wave fields. Attention is given to the hydrodynamics and wave mechanics in the model results to determine the correctness of the physical processes represented

and to explore ways in which the unstructured mesh could be optimized in order to appropriately capture the physics for both circulation and wave processes at all the different spatial scales involved. To further investigate the effect of mesh resolution on wave-induced forces and storm surge water levels a simulation is done where the unstructured ADCIRC model is coupled to a very high-resolution (30 meters) structured SWAN simulation and then compared to the results of the ADCIRC+unSWAN model. The results show that the model is in good agreement with observations, with overestimation of wave heights and water levels mostly due to overestimation of the hurricane wind fields, and that the unstructured mesh needs optimization to increase resolution in areas where wave transformation processes due to a complex bathymetry play a determinant role in the coastal dynamics.

2 Literature Review

Finite-element circulation models have been used extensively in storm surge and coastal inundation modeling (Westerink, et al. 1992; Chen, et al. 2007; Shen, et al. 2006; Dietsche, Hagen and Bacopoulos 2007; Shen, et al. 2006; Bajo, et al. 2007). These models use unstructured meshes on which resolution varies from meters to kilometers in a single mesh, thus solving motions and physical processes ranging from basin to coastal and near shore scales. The high resolution that can be achieved using these unstructured meshes allows the representation of complex structures such as reefs and irregular coastlines and the addition of high resolution datasets of land cover and surface canopies to take into account the friction forces that they impart into hydrodynamic and wind motions (Westerink, et al. 2008).

Coupling circulation and wave models introduces non-linear current-wave interactions which affect the storm surge water levels and the extent of the coastal inundation (Xie, Liu and Peng 2008).

The forces involved in these interactions include winds, tides, currents, and waves. Different coupling procedures have been used previously, each procedure focusing on the coupling of different combinations of these forces. Some studies have coupled circulation and wave models by passing the wave radiation stress forces into the circulation model to see the effect of these forces in the storm surge water levels, while other studies have included the feedback between the wave field and the wind stress into the coupling along with the radiation stresses (Funakoshi, et al. 2008; Moon,et al. 2009; Mastenbroek, et al. 1992; Brown and Wolf 2009). These studies have shown that the relative importance of each forcing on the storm surge water level is dependent on each particular location and that even at distances in the order of kilometers the dominant forcing may change due to local effects (Mastenbroek, et al. 1992). This further favors the use of unstructured meshes on which spatial resolution can be increased locally where the physical interactions requires so.

Recently the SWAN wind wave and ADCIRC circulation models were coupled into a single model on which both models run over an unstructured mesh (Dietrich, et al. 2010). In this way wave, current and water level computations are done at the same computational nodes, eliminating the need of interpolating wave forces from a structured SWAN mesh into the ADCIRC unstructured mesh and vice versa (Funakoshi, et al. 2008). Results using this coupled model show that it is in good agreement to the results when coupling a structured wave model with ADCIRC, with differences caused mainly by having a higher resolution in the structured wave model (Dietrich, et al. 2010; Bunya, et al. 2010; Dietrich, et al. 2010). Thus the unstructured coupling imposes new requirements on the refinement of unstructured meshes, as waves and current processes become important at different spatial and temporal scales (Moon, et al. 2009). New refined unstructured meshes need to include enough resolution to correctly solve both wave and current process where it is needed, but still being efficient enough to not increase resolution where it is not needed.

3 Methods

3.1 Coupled circulation and wave model

Storm surge water levels were calculated using the ADCIRC+unSWAN model (Dietrich, et al. 2010). ADCIRC+unSWAN couples the finite-element ADCIRC (Westerink, et al. 2008) shallow-water model and the spectral wind-wave SWAN model (Zijlema 2010) into a homogeneous unstructured mesh. This eliminates the need for interpolation between unstructured circulation and structured wave model grids and allows for the use of an unstructured mesh with variable resolution to capture both circulation and wave phenomena at coastal scales ranging from tens of meters to kilometers.

The ADCIRC+unSWAN coupling procedure is as follows. First the ADCIRC model runs during a determined time interval in which winds, water levels, and currents are calculated. unSWAN then accesses these winds, water levels, and currents and applies the mean over time of these variables to calculate a solution on its next time step and then calculates the radiation stress gradients. The radiation stress gradients are then passed to ADCIRC and extrapolated forward in time at every time step during the following ADCIRC stage. In this way, the radiation stress gradients are always forwarded in time in ADCIRC and winds, water levels, and currents are averaged over time in SWAN (Dietrich, et al. 2010).

3.2 ADCIRC model

The ADCIRC model solves the two-dimensional, depth-integrated shallow-water equations using a finite-element solution (Dietrich, et al. 2010, Westerink, et al. 2008). To obtain water levels the Generalized Wave Continuity Equation (Lynch and Gray 1979) is solved:

$$\frac{\partial^2 \xi}{\partial t^2} + \tau_0 \frac{\partial \xi}{\partial t} + \frac{\partial \tilde{J}_x}{\partial x} + \frac{\partial \tilde{J}_y}{\partial y} - UH \frac{\partial \tau_0}{\partial x} - VH \frac{\partial \tau_0}{\partial x} = 0 \,,$$

where:

$$\tilde{J}_x = -Q_x\frac{\partial U}{\partial x} - Q_y\frac{\partial U}{\partial y} + fQ_y - \frac{g}{2}\frac{\partial \xi^2}{\partial x} - gH\frac{\partial}{\partial x}\left[\frac{P_s}{g\rho_0} - \alpha\eta\right] + \frac{\tau_{sx,wind} + \tau_{sx,waves} - \tau_{bx}}{\rho_0}$$

$$+ (M_x - D_x) + U\frac{\partial \xi}{\partial t} + \tau_0 Q_x - gH\frac{\partial \xi}{\partial x},$$

$$\tilde{J}_y = -Q_x\frac{\partial V}{\partial x} - Q_y\frac{\partial V}{\partial y} - fQ_x - \frac{g}{2}\frac{\partial \xi^2}{\partial y} - gH\frac{\partial}{\partial y}\left[\frac{P_s}{g\rho_0} - \alpha\eta\right] + \frac{\tau_{sy,wind} + \tau_{sy,waves} - \tau_{by}}{\rho_0}$$

$$+ \left(M_y - D_y\right) + V\frac{\partial \xi}{\partial t} + \tau_0 Q_y - gH\frac{\partial \xi}{\partial y},$$

and the depth-integrated momentum equations are solved for current velocities:

$$\frac{\partial U}{\partial t} + U\frac{\partial U}{\partial x} + V\frac{\partial U}{\partial y} - fV = -g\frac{\partial}{\partial x}\left[\xi + \frac{P_s}{g\rho_0} - \alpha\eta\right] + \frac{\tau_{sx,wind} + \tau_{sx,waves} - \tau_{bx}}{\rho_0} + \frac{(M_x - D_x)}{H},$$

and:

$$\frac{\partial V}{\partial t} + U\frac{\partial V}{\partial x} + V\frac{\partial V}{\partial y} + fU = -g\frac{\partial}{\partial y}\left[\xi + \frac{P_s}{g\rho_0} - \alpha\eta\right] + \frac{\tau_{sy,wind} + \tau_{sy,waves} - \tau_{by}}{\rho_0} + \frac{\left(M_y - D_y\right)}{H}.$$

Here, U and V are depth-averaged velocities in the x- and y- directions; H=ξ+h is the total water depth; ξ is the free surface elevation minus the mean; h is the bathymetric depth; Q_x = UH and Q_y=VH are fluxes per unit width; f is the Coriolis parameter; g is the acceleration due to gravity; ρ_0 is the reference density of water; P_s is the atmospheric pressure at the surface; M are lateral stress gradients; D are momentum dispersion terms; τ_0 is a numerical parameter that optimizes the phase propagation properties; α is the effective earth elasticity factor; and η is the Newtonian equilibrium tidal potential defined as:

$$\eta(\lambda, \phi, t) = \sum_{n,j} C_{jn} f_{jn}(t_0) L_j(\phi) \cos\left[\frac{2\pi(t - t_0)}{T_{jn}} + j\lambda + v_{jn}(t_0)\right]$$

(Westerink, et al. 1992); where C_{jn} is a constant characterizing the amplitude of tidal constituent n of

species j; f_{jn} is the time dependent nodal factor; v_{jn} is the time dependent astronomical argument; j=0, 1 ,2 is the tidal species (j = 0, declinational; j = 1, diurnal; j = 2, semidiurnal); $L_0 = 3\sin^2\phi - 1$; $L_1 = \sin(2\phi)$; $L_2 = \cos^2(\phi)$; λ, ν are degrees longitude and latitude, respectively; t_0 is the reference time; and T_{jn} is the period of constituent n of species j.

The stresses $\tau_{s,winds}$, $\tau_{s,waves}$ represent the surface stresses due to winds and waves, respectively, and τ_b represents the bottom stress. The wind stress $\tau_{s,winds}$ is defined following Garrat (2007):

$$\tau_{s,winds} = C_D \rho W^2$$

where ρ is air density, W is the wind speed and C_D is a wind drag coefficient defined as:

$$C_D x 10^3 = 0.75 + 0.067W$$

where W is the wind speed at 10 meters height. This wind drag coefficient is capped at a maximum of 0.0035. Note that, though ADCIRC and unSWAN are run in a coupled mode, there is no influence of the wind waves on the sea surface wind stress which drives the wind setup component of the storm surge. As discussed at the end, this could be one of the factors limiting agreement between model and observations. The gradients of radiation stresses $\tau_{s,waves}$ are defined as:

$$\tau_{sx,waves} = -\frac{\partial S_{xx}}{\partial x} - \frac{\partial S_{xy}}{\partial y},$$

$$\tau_{sy,waves} = -\frac{\partial S_{xy}}{\partial x} - \frac{\partial S_{yy}}{\partial y},$$

where S_{xx}, S_{xy}, and S_{yy} are the radiation stresses (Longuet-Higgins and Stewart 1964) computed by the SWAN model.

3.3 SWAN wave model

SWAN is a spectral wind-wave model that computes the evolution of the wave action density N

using the action balance equation by using an iterative, point-to-point, multi-directional Gauss-Seidel based sweeping technique adapted to unstructured meshes (Zijlema 2010). The action balance equation is defined as:

$$\frac{\partial N}{\partial t} + \nabla \vec{x} \cdot \left[\left(\overrightarrow{c_g} + \vec{U} \right) N \right] + \frac{\partial c_\theta N}{\partial t} + \frac{\partial c_\sigma N}{\partial t} = \frac{S_{tot}}{\sigma} ,$$

with:

$$N(\vec{x}, t, \sigma, \theta) = E/\sigma ,$$

and:

$$S_{tot} = S_{in} + S_{wc} + S_{nl4} + S_{bot} + S_{brk} + S_{nl3}$$

Here, N is the wave action density; θ is the wave direction; σ is the relative frequency; $\overrightarrow{c_g}$ is the wave group velocity; $\vec{U}$ is the ambient current vector; c_θ and c_σ are the propagation velocities in θ-spatial and σ-spectral space; and S_{tot} are the processes that generate, dissipate or redistribute energy. These processes are the transfer of energy from wind to waves, dissipation of energy due to white capping, nonlinear transfer of wave energy due to quadruplet interaction, depth-induced breaking, and nonlinear triad interaction, respectively. The transfer of wind energy to waves is defined as:

$$S_{in}(\sigma, \theta) = A + BE(\sigma, \theta)$$

where A is the linear growth term (Cavaleri and Malanotte-Rizzoli 1981) and B is the exponential growth term (Komen, Hasselmann and Hasselmann 1984). The wind drag coefficient used in the exponential growth term is:

$$C_D x 10^3 = 0.8 + 0.065W$$

where W is the wind speed at 10 meters height (Wu 1982). This wind drag coefficient is capped at a maximum of 0.0035.

The coupling procedure requires that the gradients of radiation stresses are shared from SWAN into ADCIRC. In SWAN the wave radiation stresses are defined as:

$$S_{xx} = \rho_0 g \iint \left(\left(ncos^2\theta + n - \frac{1}{2} \right) \sigma N \right) d\sigma d\theta \,,$$

$$S_{xy} = \rho_0 g \iint (n \sin\theta \cos\theta \, \sigma N) d\sigma d\theta \,,$$

$$S_{yy} = \rho_0 g \iint \left(\left(nsin^2\theta + n - \frac{1}{2} \right) \sigma N \right) d\sigma d\theta \,,$$

where n is the ratio of group velocity over phase speed.

3.4 Parametric wind model

Hurricane wind fields were generated using the parametric Holland (1980) model. This model calculates a symmetric wind field V_g depending on the radius of maximum winds R_{max}, central pressure p_c, ambient pressure p_n, air density ρ, and the distance r from the hurricane's center:

$$V_g(r) = \sqrt{\frac{AB(p_n - p_c)e^{-\frac{A}{r^B}}}{\rho r^B} + \frac{r^2 f^2}{4}} - rf/2$$

where:

$$A = {R_{max}}^B$$

and the B parameter has various formulations. In this case two formulations are used, one in which the B parameter is determined by the maximum wind speed V_{max} as defined by (Phadke, et al. 2003):

$$B = \frac{V_{max}\, \rho e}{p_{c-} p_n}$$

and the other is not dependent on the maximum wind speed (Holland 2008):

$$B = -4.4x10^{-5} * dp^2 + 0.01 * dp + 0.03 * \frac{\partial p_c}{\partial t} - 0.014\varphi + 0.15{V_T}^x + 1.0$$

$$where: x = 0.6 * (1 - \frac{dp}{215})$$

where dp is the difference between ambient and central pressure, φ is the hurricane's center latitude and V_T is the hurricane's translation speed. The radius of maximum winds follows Hsu and Yan (1998), who determined a radius of maximum winds for each hurricane category based on historical hurricane data. On the simulations the central pressure of each hurricane was used to determine its corresponding hurricane category and assign the appropriate R_{max}. Asymmetry is introduced in the model by adding the vectorial translation velocity to the parametric wind field (Peng, Xie and Pietrafesa 2006):

$$\overrightarrow{V_{assym}(r)} = \overrightarrow{V_g(r)} + \overrightarrow{V_T}$$

where $\overrightarrow{V_g(r)}$ and $\overrightarrow{V_T}$ are the vector components of the hurricane wind field $V_g(r)$ and the hurricane's translation velocity. This $\overrightarrow{V_{assym}(r)}$ asymmetric wind field is then used to force the ADCIRC, unSWAN, and SWAN models.

3.5 Computational domain

3.5.1 ADCIRC+unSWAN

For the coupled ADCIRC+unSWAN model simulations the unstructured mesh created for the 2007 FEMA Flood Insurance Study was used. This mesh has 124,815 nodes and 242,976 triangular elements, and its spatial resolution ranges from 60 kilometers at the boundaries to a maximum of 50 meters at the San Juan harbor. This range in resolution illustrates the advantages that an irregular grid provides in the ability of solving phenomena at numerous scales without the need of using nested grids and interpolation between areas of interest. Figure 1 and Figure show the ADCIRC+unSWAN computational domain and a detail of the mesh at the San Juan harbor, respectively.

3.5.2 ADCIRC and structured SWAN coupling

To explore the effects of mesh resolution on SWAN on areas of highly complex bathymetry a structured mesh was created for the area of La Parguera in the southwestern area of Puerto Rico. The

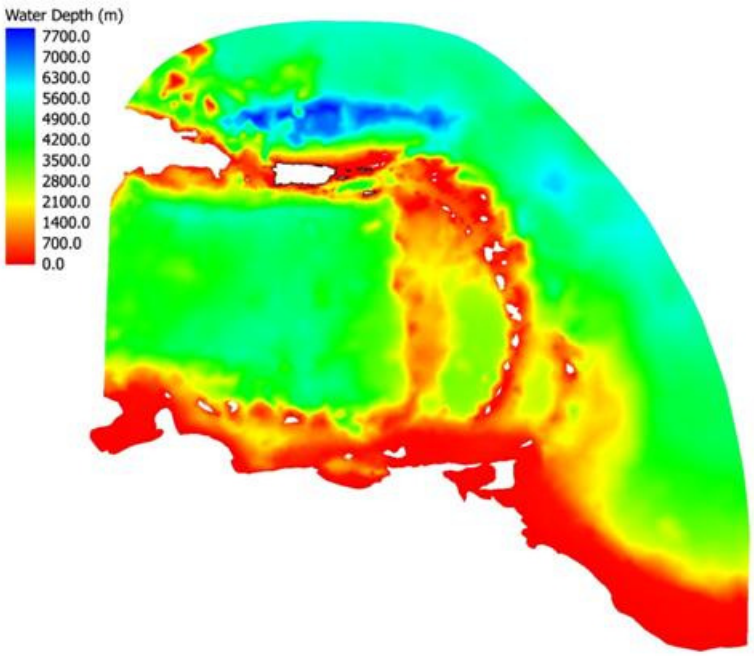

Figure 1. Water depths (m) on ADCIRC+unSWAN computational domain.

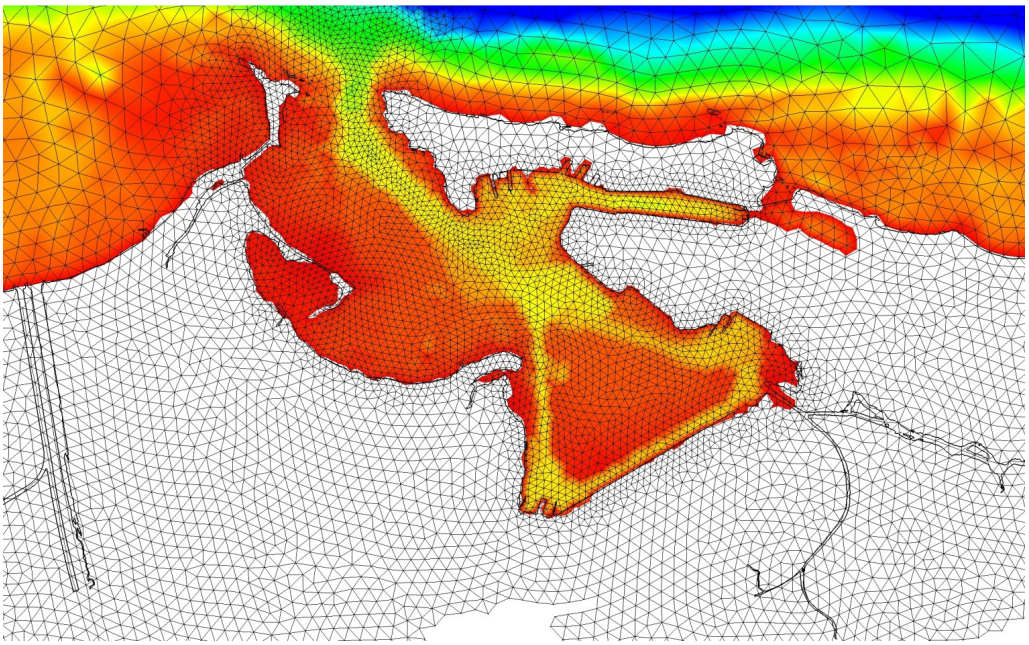

Figure 2. Detail of ADCIRC+unSWAN mesh at San Juan harbor. Color shading is according to water depth.

structured mesh had a resolution of 30 meters and bathymetric data was provided by the National Geophysical Data Center (National Geophysical Data Center 2010). This high resolution mesh was nested inside a coarser 5 kilometer resolution mesh with bathymetric data from the ETOPO1 global relief model (Amante and Eakins 2009). Figure 3 shows La Parguera on the unstructured mesh with a maximum resolution of 200 meters and Figure 4 shows the high resolution structured grid with a resolution of 30 meters in La Parguera. The improvement in detail over features like reefs, small islands and the coastline is clearly seen on the high resolution grid.

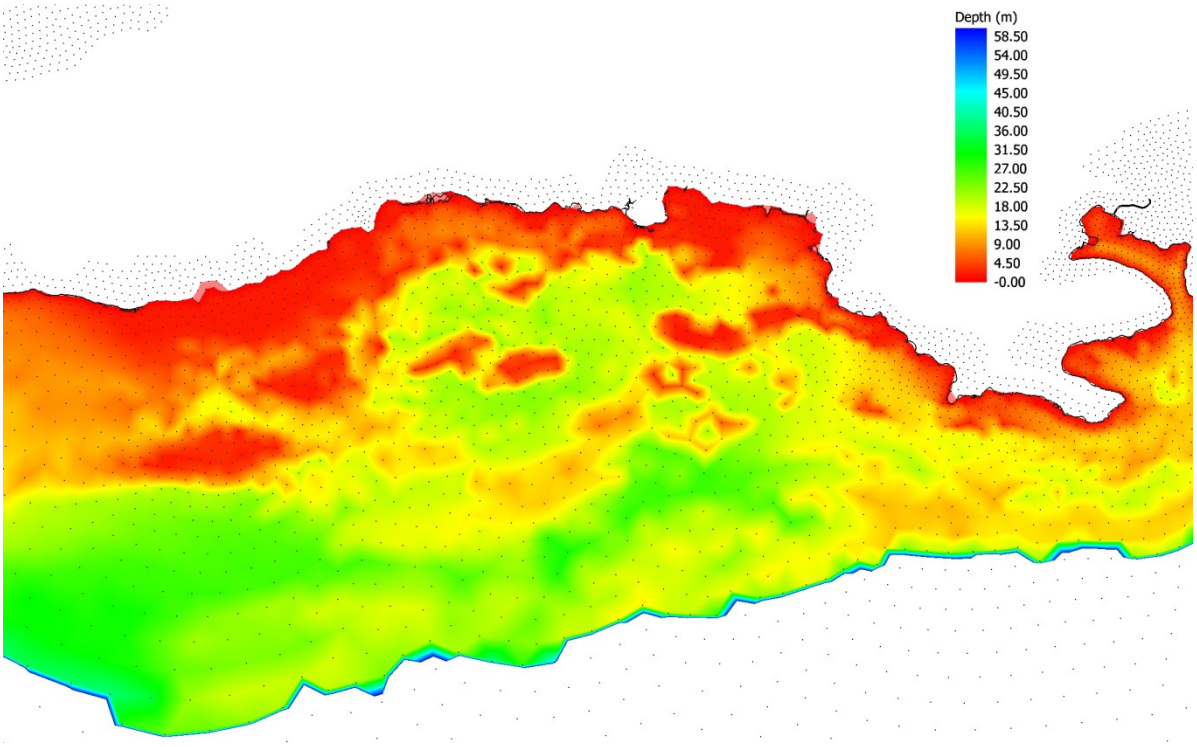

Figure 3. Details of water depth (0-60 m contours) in La Parguera on the unstructured mesh.

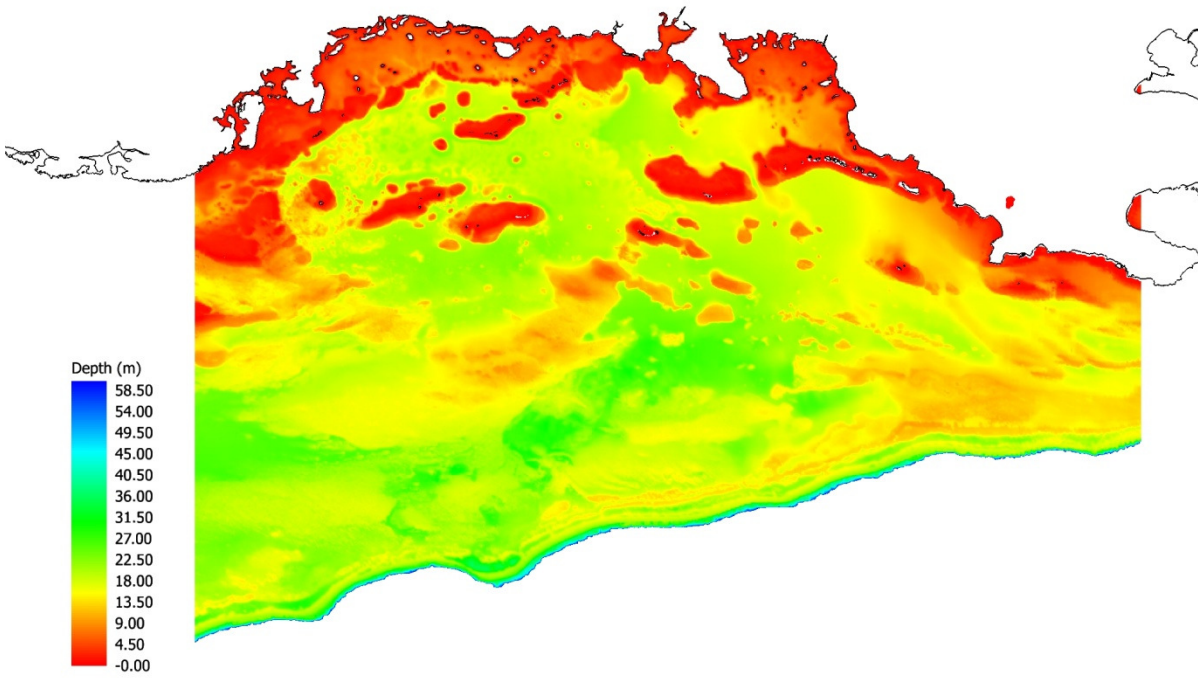

Figure 4. Details of water depth (0-60 m contours) in La Parguera on the high resolution structured mesh.

3.6 Model setup

During all simulations ADCIRC ran at a time step of 1 second,-with all time and spatial non-linear terms activated. Wetting and drying was allowed so flooding could occur over inland nodes in the mesh. Bottom friction was parameterized using a hybrid friction relationship (Westerink, et al. 2008) in which a Manning-type friction law is applied for depths shallower than 2 meters and for deeper waters a standard Chezy friction law is used. New coordinates for the hurricane's center were updated every 6 hours from the data provided by the HURDAT (Landsea 2010) database.

For purposes of this thesis we will use the convention of ADCIRC+unSWAN whenever we are

running ADCIRC coupled with the unstructured version of SWAN (unSWAN). When coupled with the structured version of SWAN we will refer to it as ADCIRC+SWAN. For the each coupling the SWAN and unSWAN wave models had different time step configurations. In the ADCIRC+unSWAN coupling unSWAN had a time step of 10 minutes, while for the ADCIRC+SWAN coupling the SWAN time step was 15 minutes. SWAN has an implicit numerical formulation so this difference in time steps is due to computational time constraints and the time scales of the physical processes involved. Both time steps follow values used in previous studies where both coupling procedures were used (Dietrich, et al. 2010; Funakoshi, et al. 2008).

The ADCIRC+unSWAN simulations had a coupling interval of 10 minutes for winds, currents, water levels, and radiation stresses (that is, data was shared between models every 10 simulation minutes). This coupling includes all computational nodes in the mesh, but for the unSWAN computations refraction was limited to depths below 20 meters to avoid numerical instabilities due to steep bathymetry at the shelf breaks (Dietrich, et al. 2010), which was not well resolved by the unstructured mesh. It should be noted that the unstructured mesh was originally made for modeling storm surge inundations due solely to hurricane winds, without wave forcing. The twenty meters isobath lies shoreward of the shelf break.

When coupling the structured SWAN model and ADCIRC, winds, currents, and water levels were passed to SWAN at one hour intervals, then radiations stresses were calculated in SWAN and passed back to ADCIRC. Radiation stresses were calculated only in the structured SWAN high resolution nested domain area as this was the only location of interest for exploring the effect of mesh resolution. The coupling interval was determined following Funakoshi, et al. (2008), who found that the model response did not change for coupling intervals between one and four hours, and that the coupling interval should then depend on the available computing resources.

4 Results

4.1 Tidal Validation

To verify the model's hydrodynamics performance a tide-only simulation was conducted for both Hurricane Georges and Hurricane Omar. The model was forced at the open boundaries with eight tidal constituents: K_1, O_1, P_1, Q_1, N_2, M_2, S_2, and K_2. The elevation forcing for these constituents were obtained from the TOPEX/Poseidon Global Inverse Solution TPXO (E.G. Egbert, et al. 1994). In order to reference the tidal solution to the dates of interest the nodal factor and equilibrium argument for each tidal constituent were included. Table 1 and

Table 2 show the appropriate nodal factor and equilibrium arguments for each simulation. For both simulations the model had a spin-up time of 45 days and a total length of 60 days. Only the last 15 days of each simulation were taken into consideration for the comparisons.

To avoid atmospheric influences and measurement errors in quantifying the model performance, the model solution was compared to the harmonic tide prediction at selected NOAA tide stations instead of observed tide records.

Table 1. Principal tidal constituents, nodal factors and equilibrium arguments used for Hurricane Georges simulation. Nodal factors and equilibrium arguments were calculated for a 60 day period starting on August 1, 1998.

Constituent	Nodal Factor	Equilibrium Argument (deg)
K1	0.9	214.44
O1	0.84	313.29
P1	1	140.59
Q1	0.84	112.51
N2	1.03	324.27
M2	1.03	165.04
S2	1	0
K2	0.78	249.68

Table 2. Principal tidal constituents, nodal factors and equilibrium arguments used for Hurricane Omar simulation. Nodal factors and equilibrium arguments were calculated for a 60 day period starting on August 21, 2008.

Constituent	Nodal Factor	Equilibrium Argument (deg)
K1	1.09	245.17
O1	1.14	6.91
P1	1	120.31
Q1	1.14	58.42
N2	0.97	305.84
M2	0.97	254.33
S2	1	0
K2	1.23	310.9

For the stations in which they were available (San Juan, Magueyes Island, and Charlotte Amalie) an average seasonal cycle correction was made to the model solution by adding the seasonal height correction to the modeled tide elevation. Figure 5 to Figure 7 show the average seasonal cycles for these stations. Due to unavailability of data only two stations were used for the comparisons for the Hurricane Georges simulation, compared to the Hurricane Omar simulation where six stations were used.

Four difference statistics were used to quantify the model's performance in predicting the tides: mean, standard deviation, mean absolute error and root mean square error. The mean absolute error is defined as:

$$\frac{\sum_{i=1}^{N}|A_i - H_i|}{N}$$

and the root mean square error is defined as:

$$\frac{\sum_{i=1}^{N}\sqrt{(A_i - H_i)^2}}{N}$$

where A is the ADCIRC predicted surface elevation in meters, H is the harmonic prediction in meters, and N is the total simulation length. For both simulations N = 360 hours.

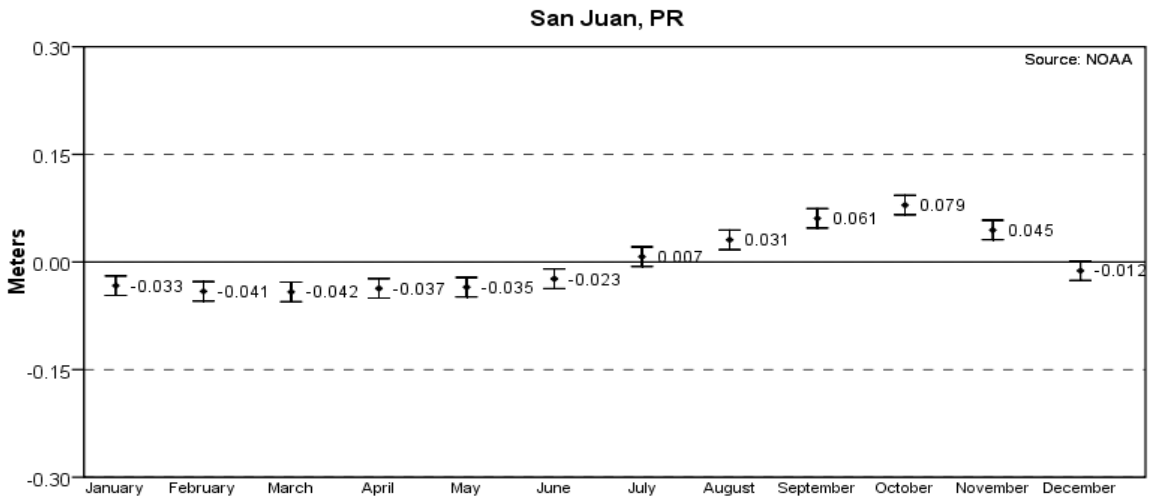

Figure 5. Average seasonal cycle for the San Juan station.

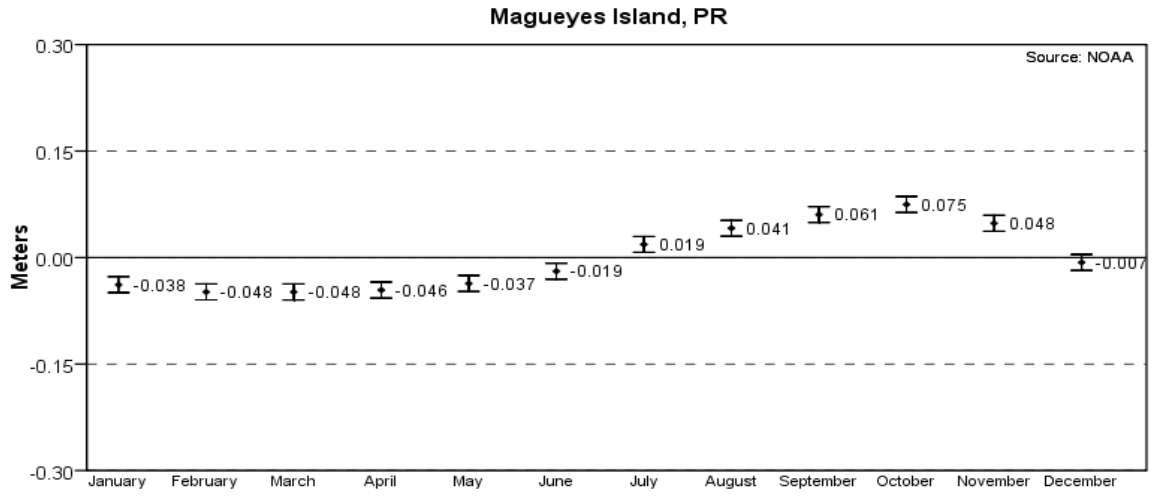

Figure 6. Average seasonal cycle for the Magueyes Island station.

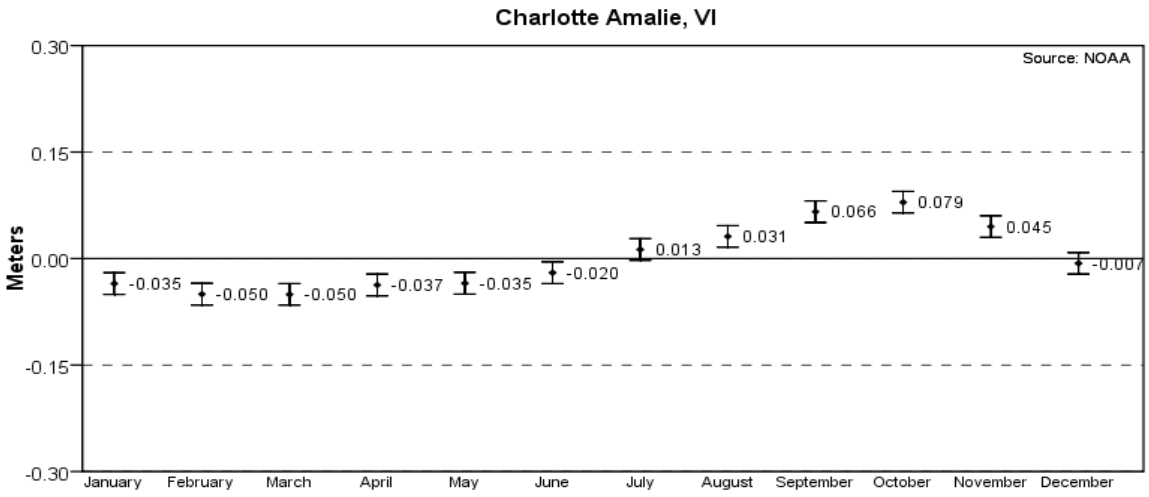

Figure 7. Average seasonal cycle for the Charlotte Amalie station.

Results for the tidal simulation for the Hurricane Georges period are shown in Figure 8 and Figure 9. It can be seen that the model correctly predicts the semi-diurnal and mixed semi-diurnal cycles at San Juan and the diurnal cycle at Magueyes Island, while it has some difference in the mixed-diurnal at Magueyes Island from September 20 to September 23. This difference may be accounted by the model's bathymetry given that the tidal range during these days was in the range of less than 0.1 meters. Table 3 shows the difference statistics for this simulation and it is clear that the model correctly predicted the tidal elevation for the time period for both stations.

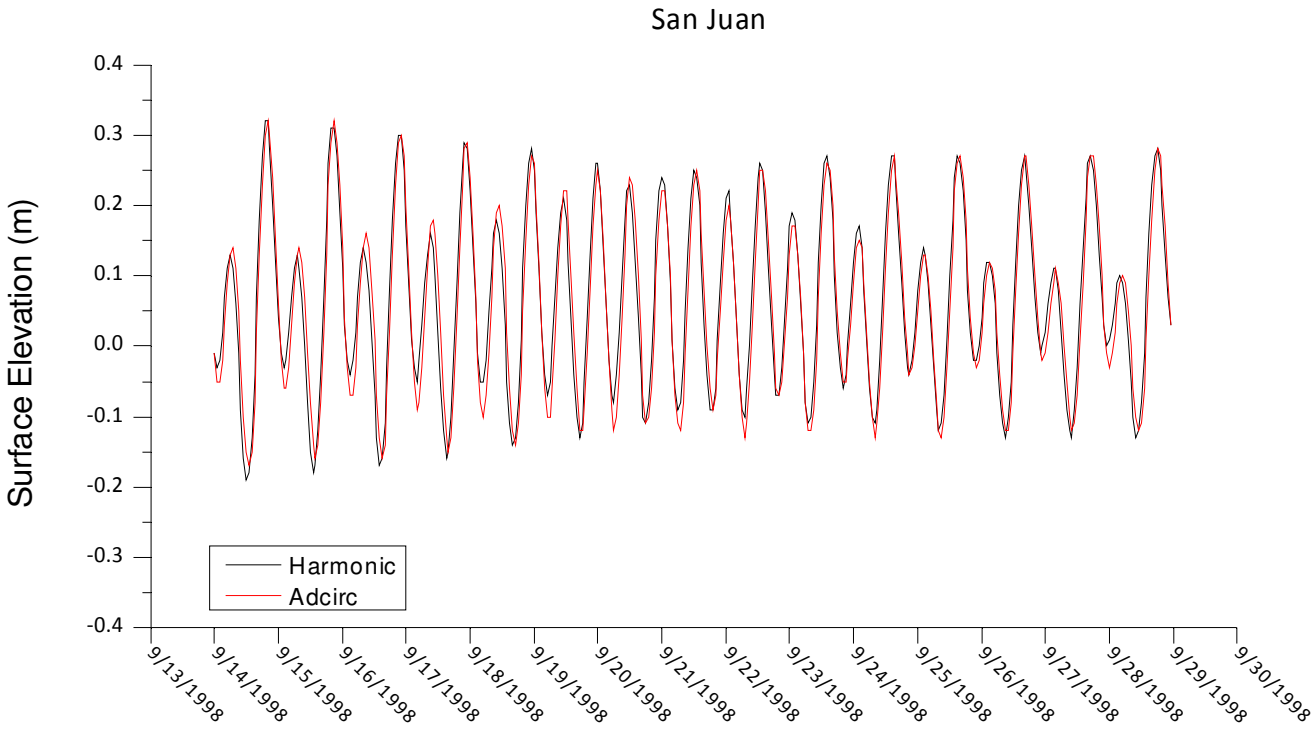

Figure 8. Surface elevation during the tidal simulation from September 14, 1998 to September 29, 1998 at the San Juan station.

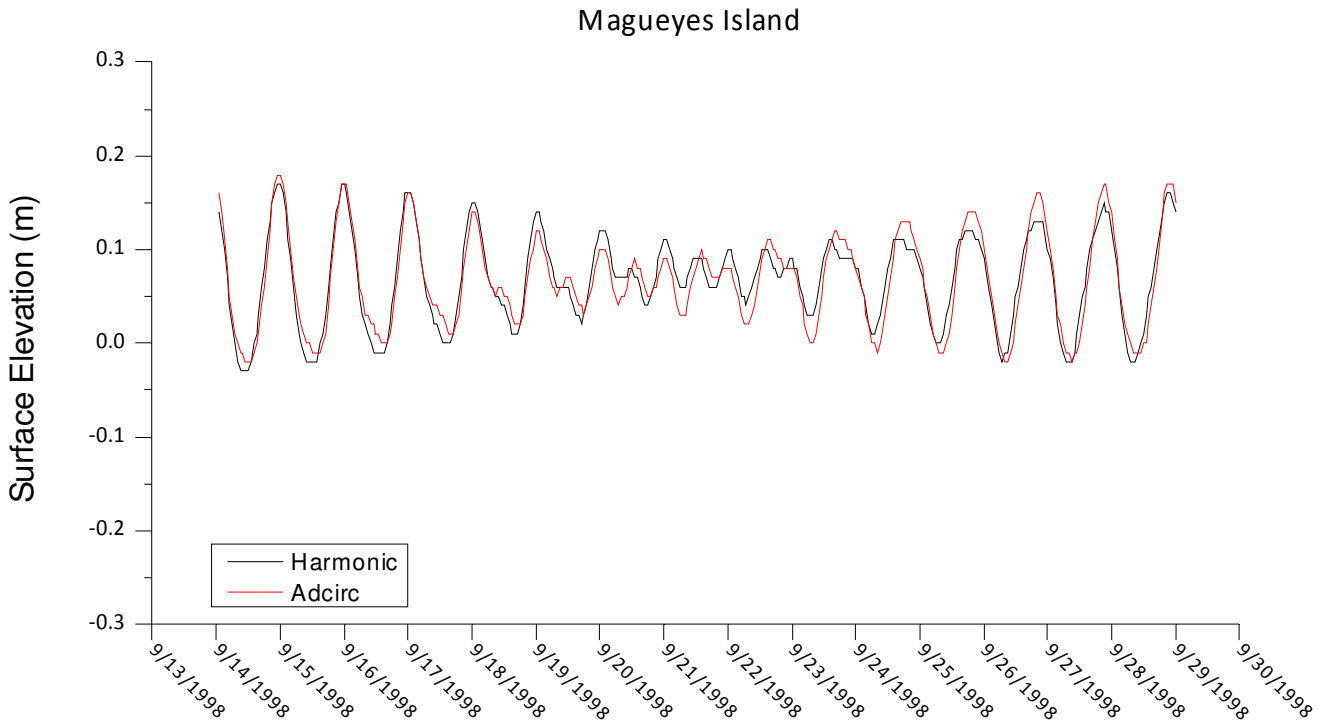

Figure 9. Surface elevation during the tidal simulation from September 14, 1998 to September 29, 1998 at the Magueyes Island station.

Table 3. Difference statistics for surface elevation (m) for the 15 day (September 14, 1998 – September 29, 1998) tidal simulation. Harmonic refers to NOAA harmonic predictions while Adcirc refers to the model prediction.

Station	MAE (m)	RMSE (m)	Mean Harmonic (m)	Mean Adcirc (m)	Std Dev Harmonic (m)	Std Dev Adcirc (m)
San Juan	0.0289	0.0347	0.0654	0.0601	0.1241	0.1248
Magueyes	0.0145	0.0168	0.0682	0.0671	0.0485	0.0501

Figure 10 to Figure 15 show the tidal simulation results for the Hurricane Omar period. The model correctly predicts the diurnal and semi-diurnal cycles at all stations while some difference is seen for the mixed-diurnal cycle at Magueyes Island, Vieques Island, Culebra Island, Charlotte Amalie, and Christiansted Bay. As in the case for the mixed-diurnal cycle during Hurricane Georges' period this difference may be accounted by the model's bathymetry as the tidal range during this cycles were in the range of less than 0.1 meters. Table 4 shows the difference statistics for this simulation and it is clear that the model correctly predicted the tidal elevation for the time period for both stations.

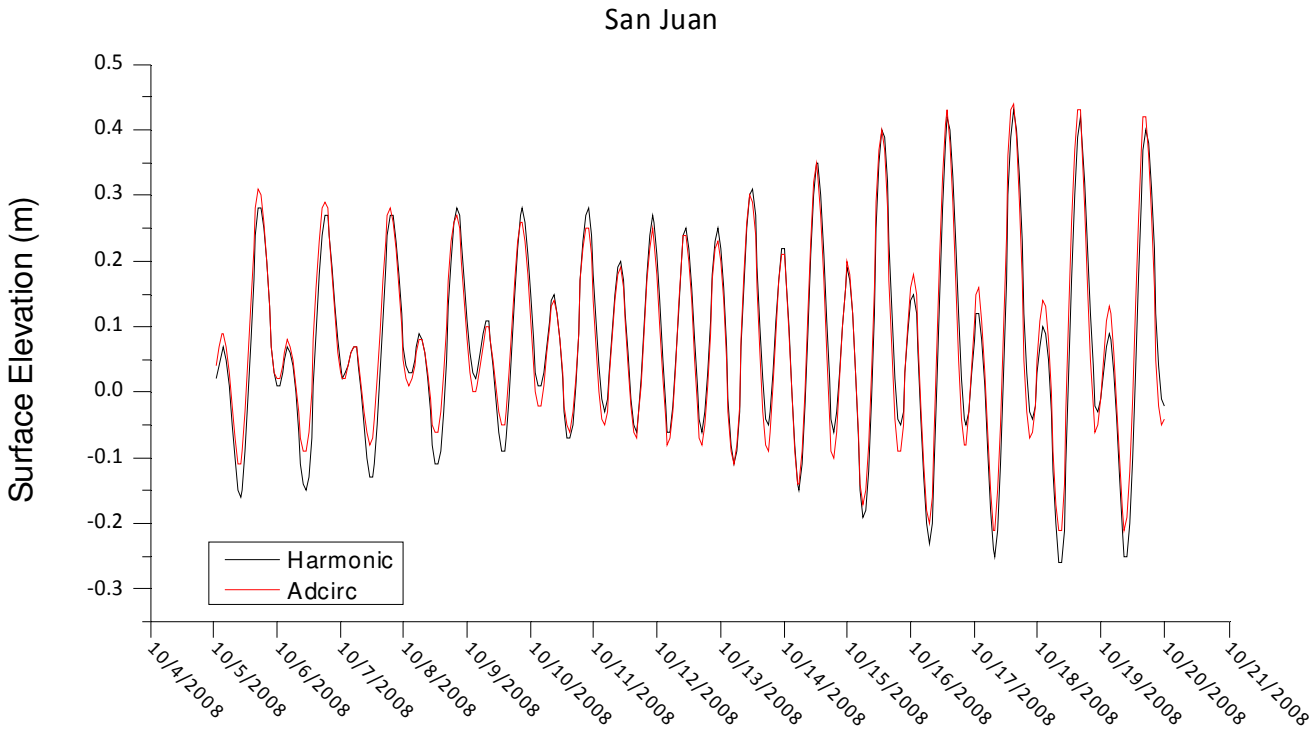

Figure 10. Surface elevation during the tidal simulation from October 5, 2008 to October 20, 2008 at the San Juan station.

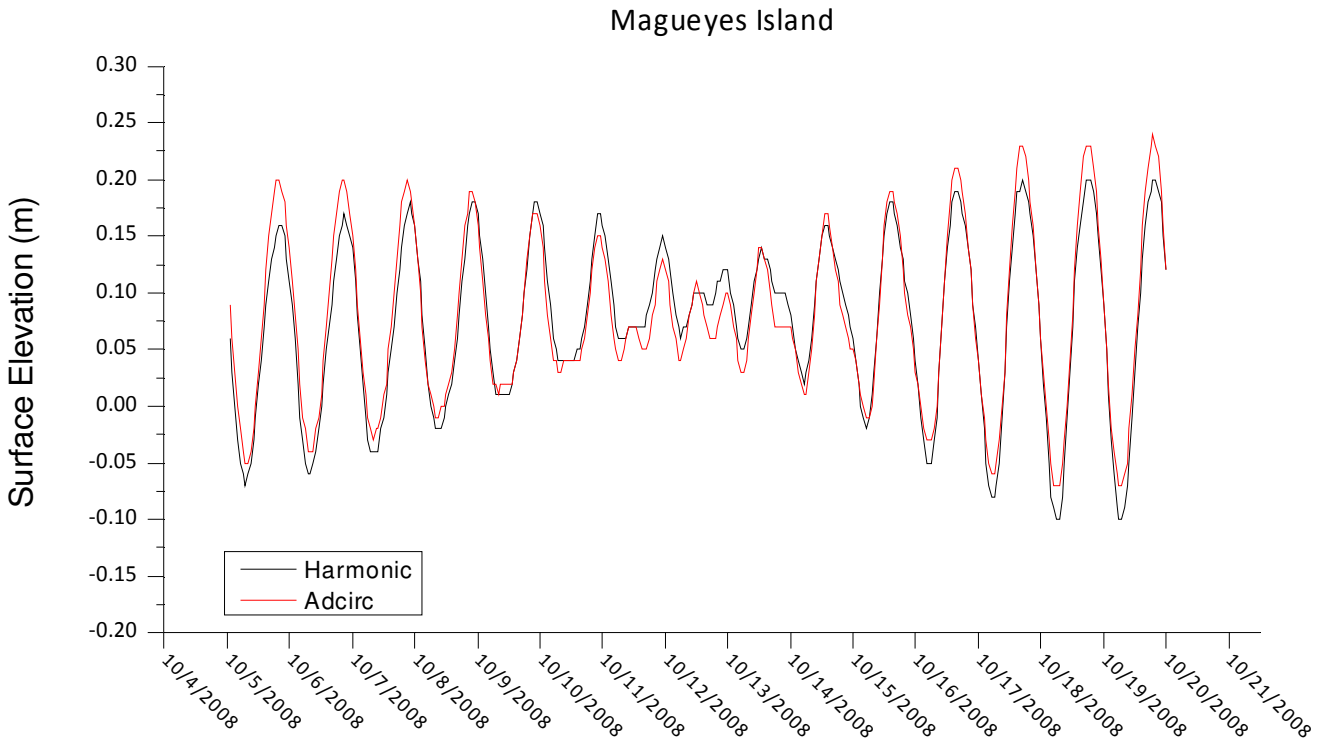

Figure 11. Surface elevation during the tidal simulation from October 5, 2008 to October 20, 2008 at the Magueyes Island station.

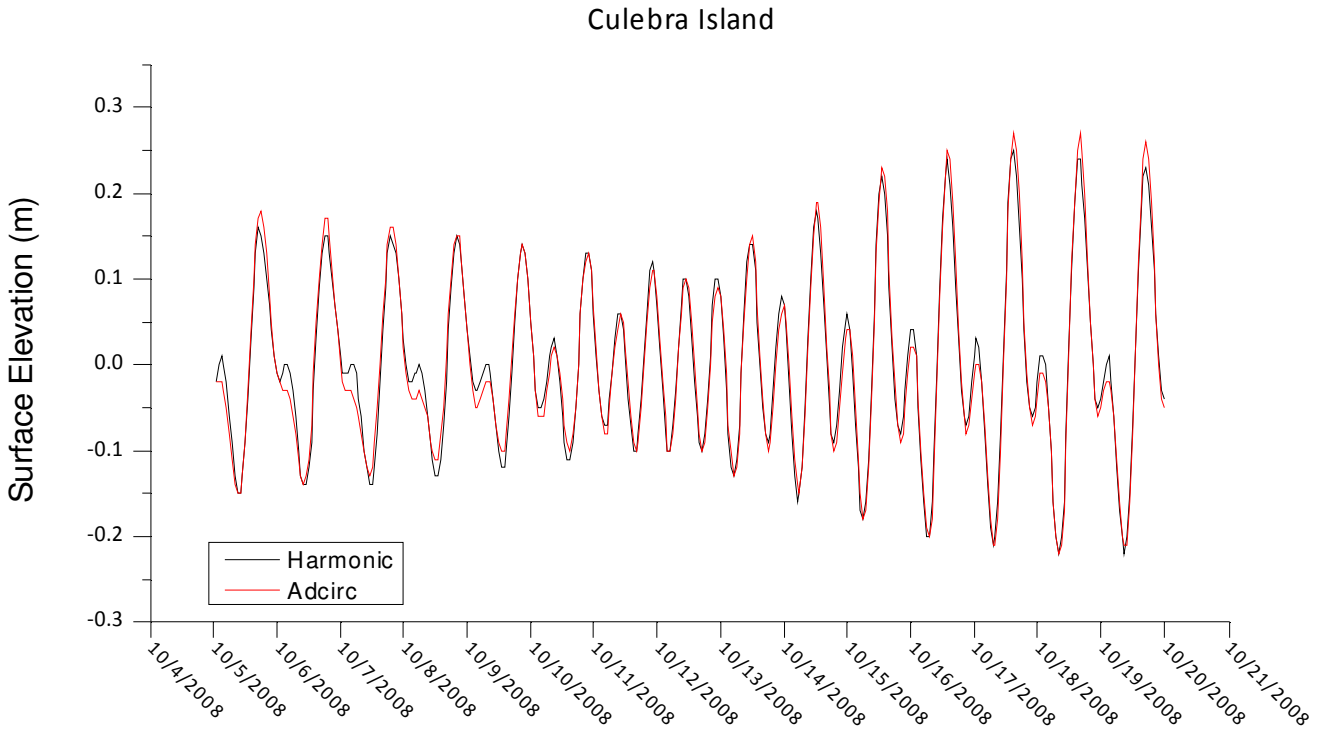

Figure 12. Surface elevation during the tidal simulation from October 5, 2008 to October 20, 2008 at the Culebra Island station.

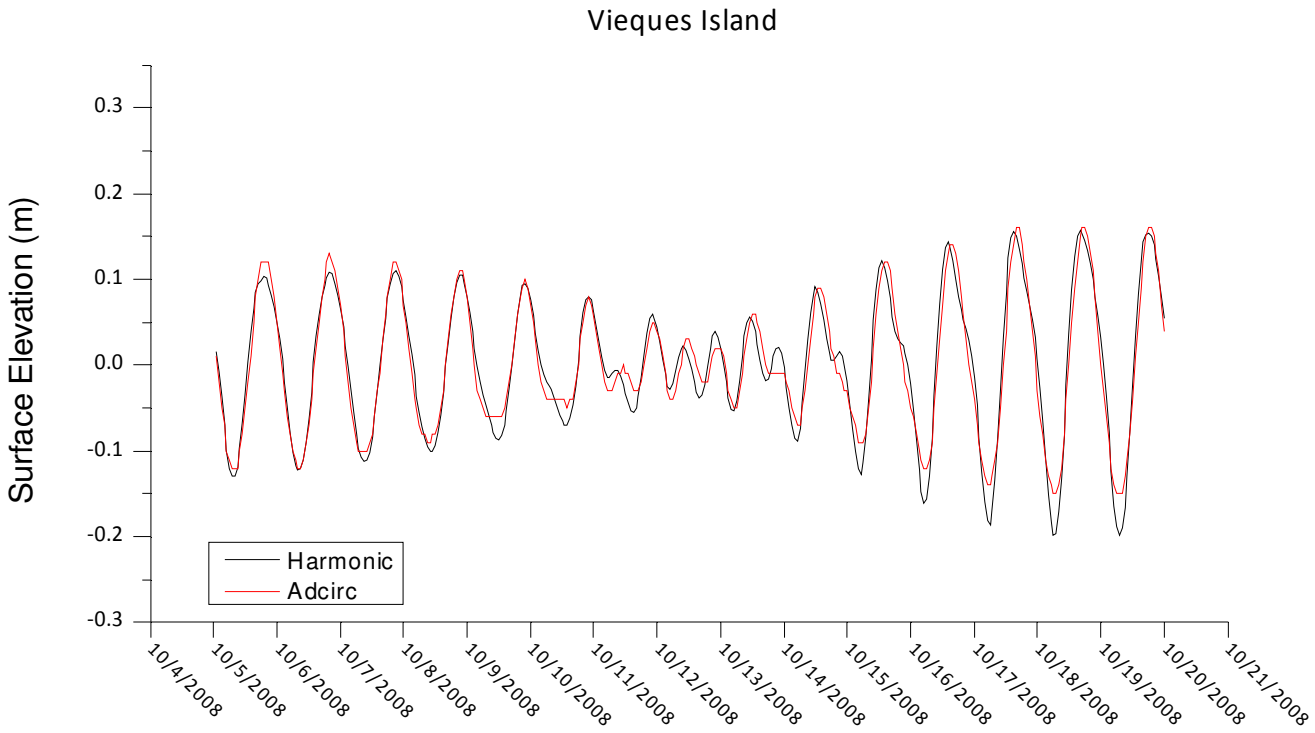

Figure 13. Surface elevation during the tidal simulation from October 5, 2008 to October 20, 2008 at the Vieques Island station.

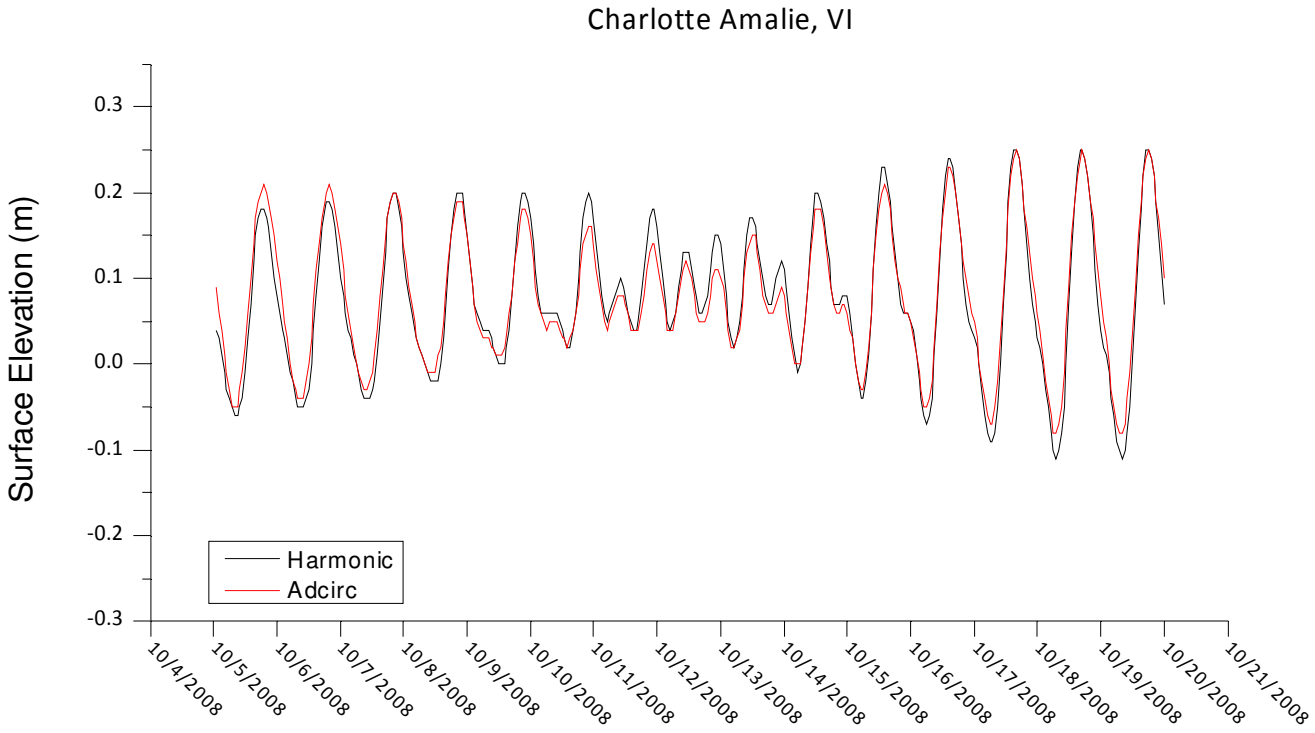

Figure 14. Surface elevation during the tidal simulation from October 5, 2008 to October 20, 2008 at the Charlotte Amalie station.

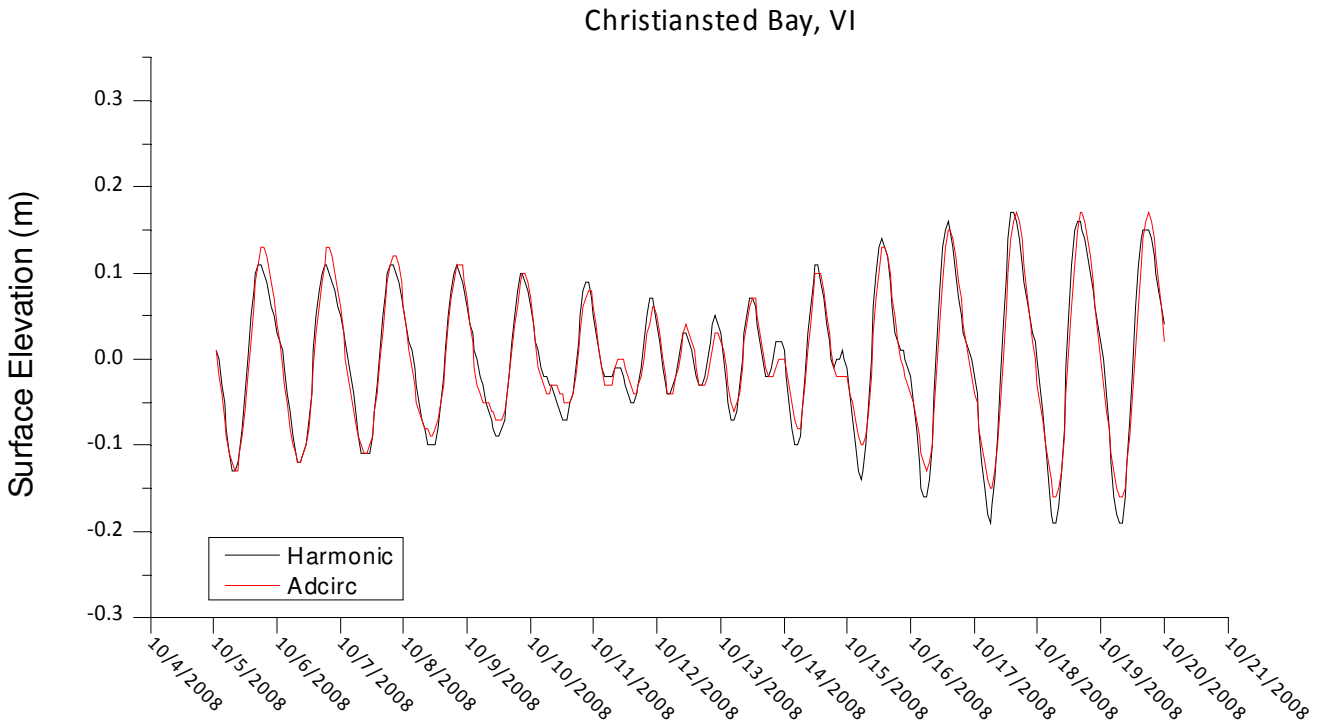

Figure 15. Surface elevation during the tidal simulation from October 5, 2008 to October 20, 2008 at the Christiansted Bay station.

Table 4. Difference statistics for surface elevation (m) for the 15 day (October 5, 2008 – October 20, 2008) tidal simulation. Harmonic refers to NOAA harmonic predictions while Adcirc refers to the model prediction.

Station	MAE (m)	RMSE (m)	Mean Harmonic (m)	Mean Adcirc (m)	Std Dev Harmonic (m)	Std Dev Adcirc (m)
San Juan	0.0279	0.0348	0.0743	0.0793	0.1482	0.1428
Magueyes	0.0161	0.0195	0.0744	0.0792	0.0744	0.0746
Culebra	0.0125	0.0157	0.0004	0.0003	0.1018	0.1056
Vieques	0.0159	0.0195	0.0005	0.0004	0.0812	0.0764
Charlotte Amalie	0.0154	0.0192	0.0771	0.0795	0.0856	0.0785
Christiansted Bay	0.0146	0.0182	0.0009	0.0002	0.0822	0.0785

4.2 Parametric wind model

The formulations for the B parameter given by Phadke, et al. (2003) and Holland (2008) result in different values for the parameter in both Hurricane Georges and Hurricane Omar. Table 5 and Table 6 show the B parameter values at six hour intervals for each hurricane. In the case of Hurricane Georges the Phadke et al. (2003), formulation resulted in higher B parameter values, while in the Hurricane Omar case the Holland (2008) formulation resulted in higher B parameter values. As described in Holland (1980), the B parameter determines the shape of the wind profile, that is, the spread and magnitude of the maximum wind speed relative to the hurricane's radius of maximum winds. To adequately illustrate the effect of the B parameter on the hurricane's wind field the model's wind result must be compared to observed winds during the studied hurricanes.

Wind observations were obtained from NOAA's National Data Buoy Center and National Ocean Service buoys and meteorological stations. Data records for Hurricane Georges and Hurricane Omar span the same time period as the simulations in order to picture the observations response to the hurricane's effects and up to what extent the parametric wind model replicates them. During Hurricane Georges only the Luis Munoz Marin International Airport had wind observations for all the simulation period and this data was obtained from NOAA's National Climatic Data Center.

As the parametric wind model does not take into account topographic factors and the computational mesh does not includes wind reduction factors such as the terrain roughness length, all wind observations were adjusted as to be under marine exposure (Westerink, et al. 2008) and referenced to a 10 meter height and 1-minute average sustained wind, which is the HURDAT convention. To adjust the observed winds the procedure proposed by Powell and Houston (1996) was used, where wind observations U_z at height Z are adjusted to a 10 meter height following the logarithmic law:

Table 5. Asymmetric parametric wind equation's (Peng, Xie and Pietrafesa 2006) B parameter as calculated using Phadke, et al. (2003) and Holland (2008) methods for Hurricane Georges. Latitude and longitude are the hurricane's center at 6 hour intervals.

Longitude (degrees)	Latitude (degrees)	Phadke, et al.	Holland
-60.60°	16.70	1.590710	1.749364
-62.10	17.10	1.688100	1.627822
-63.60	17.40	1.523510	1.530949
-65.00	17.80	1.558156	1.673897
-66.30	18.20	1.488904	1.423740
-67.40	18.00	1.736093	1.504126
-68.50	18.20	1.788145	1.234923
-69.70	18.60	1.658933	1.645356
-70.80	18.80	1.158037	1.694228

Table 6. Asymmetric parametric wind equation's (Peng, Xie and Pietrafesa 2006) B parameter as calculated using Phadke, et al. (2003) and Holland (2008) methods for Hurricane Omar. Latitude and longitude are the hurricane's center at 6 hour intervals.

Longitude (degrees)	Latitude (degrees)	Phadke, et al.	Holland
-69.6000	14.5000	1.0000	1.0506
-69.3000	14.3000	1.0000	1.0563
-69.1000	14.2000	1.0000	1.0000
-68.8000	13.9000	1.0000	1.0639
-68.3000	14.1000	1.0921	1.3300
-68.0000	14.4000	1.3510	1.3433
-67.4000	14.9000	1.5009	1.3356
-66.5000	15.6000	1.3931	1.2476
-65.2000	16.7000	1.6589	1.3372
-63.9000	18.2000	1.9192	1.2302
-62.1000	19.6000	1.6750	2.0646
-60.4000	21.1000	1.3510	1.7984
-58.8000	22.8000	1.2051	1.5090

$$\frac{U_{10}}{U_z} = \frac{\ln\left[\frac{(10 - Z_D)}{Z_0}\right]}{\ln\left[\frac{(Z - Z_D)}{Z_0}\right]}$$

Open water was given a roughness length (Z_0) of 0.01 m (Powell and Houston 1996) and Z_0 for each meteorological station was estimated using the parameters given by Steyaerd and Knox (2008). Table 7 shows the anemometer height and roughness length values for each station. The wind observations were adjusted from the instrument averaging period to a 1-minute average sustained wind using the conversion proposed by Powell and Houston (1996):

$$G_{60,T} = 2.6631 - 2.1244 \log \mathrm{T} + 0.85245 (\log \mathrm{T})^2 - 0.10346 (\log \mathrm{T})^3$$

where T is the wind averaging period (seconds) for the meteorological observations. The averaging period for each station are shown in Table 7.

Results for Luis Munoz Marin International airport during Hurricane Georges are shown in Figure 16. Both B parameter formulations result in a similar wind profile for both wind speed and direction. Table 8 shows that the Holland (2008) B formulation predicts the maximum wind speed better than Phadke, et al. (2003) when compared to the adjusted observed wind

Table 7. Station name, location, roughness length parameter, averaging period, and anemometer height for the meteorological stations. Roughness length values follow Steyaerd and Knox (2008)

Station	Longitude (degrees)	Latitude (degrees)	Z_0 (m)	Averaging period (min)	Anemometer Height (m)
Luis Munoz Marin Intl. Airport	-66.0000	18.4330	0.05	2	6.4
Buoy 42059	-67.4960	15.0060	0.01	10	5.0
Charlotte Amalie, VI	-64.9200	18.3350	0.80	2	4.6
Christiansted Bay, VI	-64.6990	17.7480	0.20	2	6.7
Lime Tree Bay, VI	-64.7530	17.6970	0.15	2	3.0

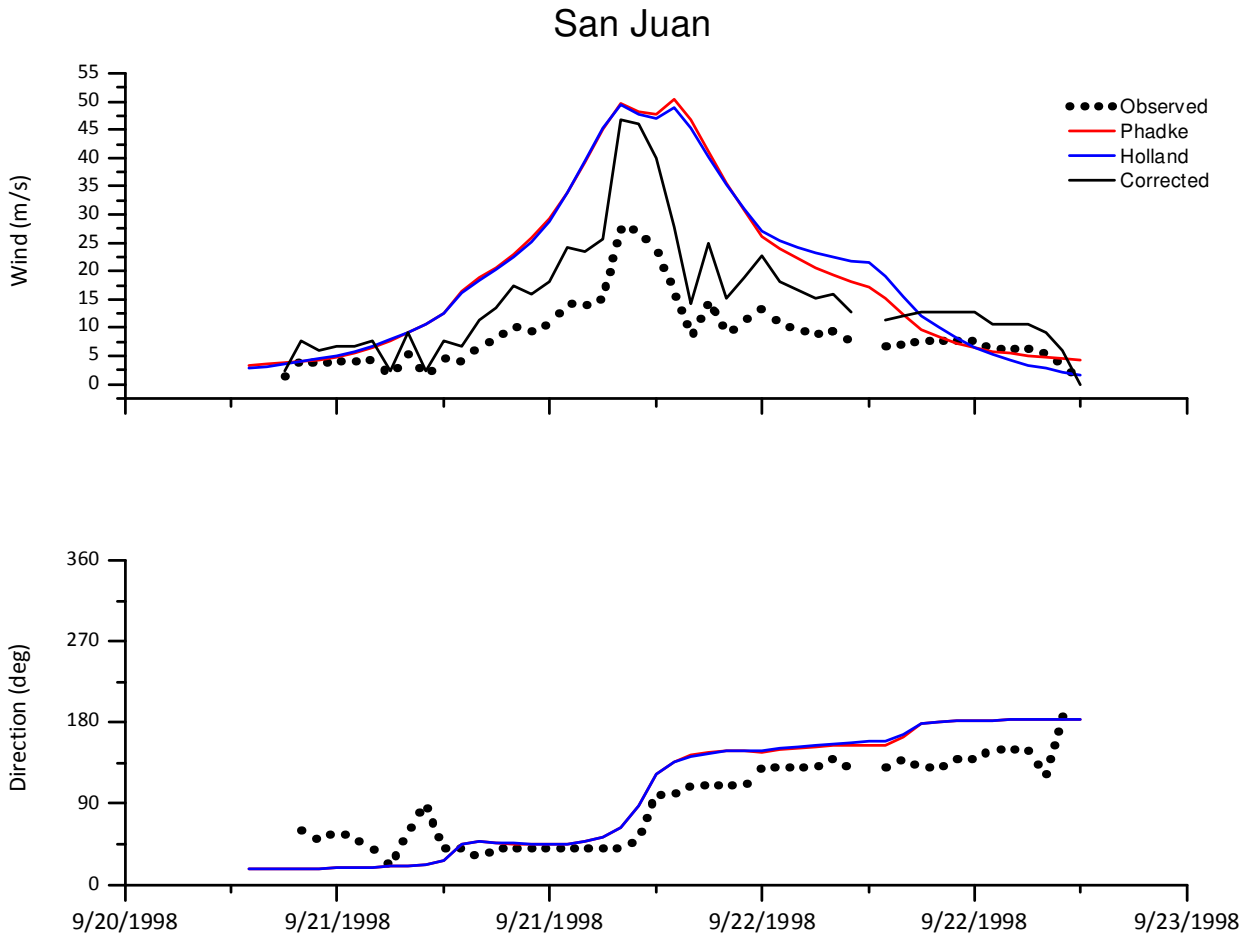

Figure 16. 10-meter wind speed (m/s) and direction (meteorological convention) during Hurricane Georges at Luis Munoz Marin International Airport. The observed wind speed represents the data measured by the instrument; the corrected wind speed represents the observed wind speed adjusted to marine exposure and 1-minute average.

Table 8. Maximum wind speed (m/s) for the observed, adjusted, and parametric winds calculated with each respective B parameter formulation. – indicates that no data was available.

	Hurricane Georges				Hurricane Omar			
Station	Observed	Corrected	Phadke, et al.	Holland	Observed	Corrected	Phadke, et al.	Holland
Luis Munoz Marin Intl. Airport	27.714	46.82	50.51	49.54	-	-	-	-
Buoy 42059	-	-	-	-	26.00	32.08	33.39	31.68
Charlotte Amalie, VI	-	-	-	-	6.80	26.89	34.06	29.76
Christiansted Bay, VI	-	-	-	-	22.90	45.11	49.39	40.15
Lime Tree Bay, VI	-	-	-	-	21.70	50.10	47.55	39.54

speed. It is clear that by adjusting the observed winds to a marine exposure, which is equivalent to removing the land roughness effect from the observed winds, the maximum parametric winds closely predict the maximum adjusted observed winds. The changes in wind direction are well represented by both B parameter formulations, with no noticeable differences between them.

During Hurricane Omar there were more observations available so a better assessment of the parametric wind model can be made. Figure 17 - Figure 20 show the wind speed and direction at NDBC Buoy 42059, Charlotte Amalie, Christiansted Bay, and Lime Tree Bay respectively. All figures indicate that the Holland (2008) B parameter formulation results in lower maximum winds. The wind speed direction shows a difference between both B

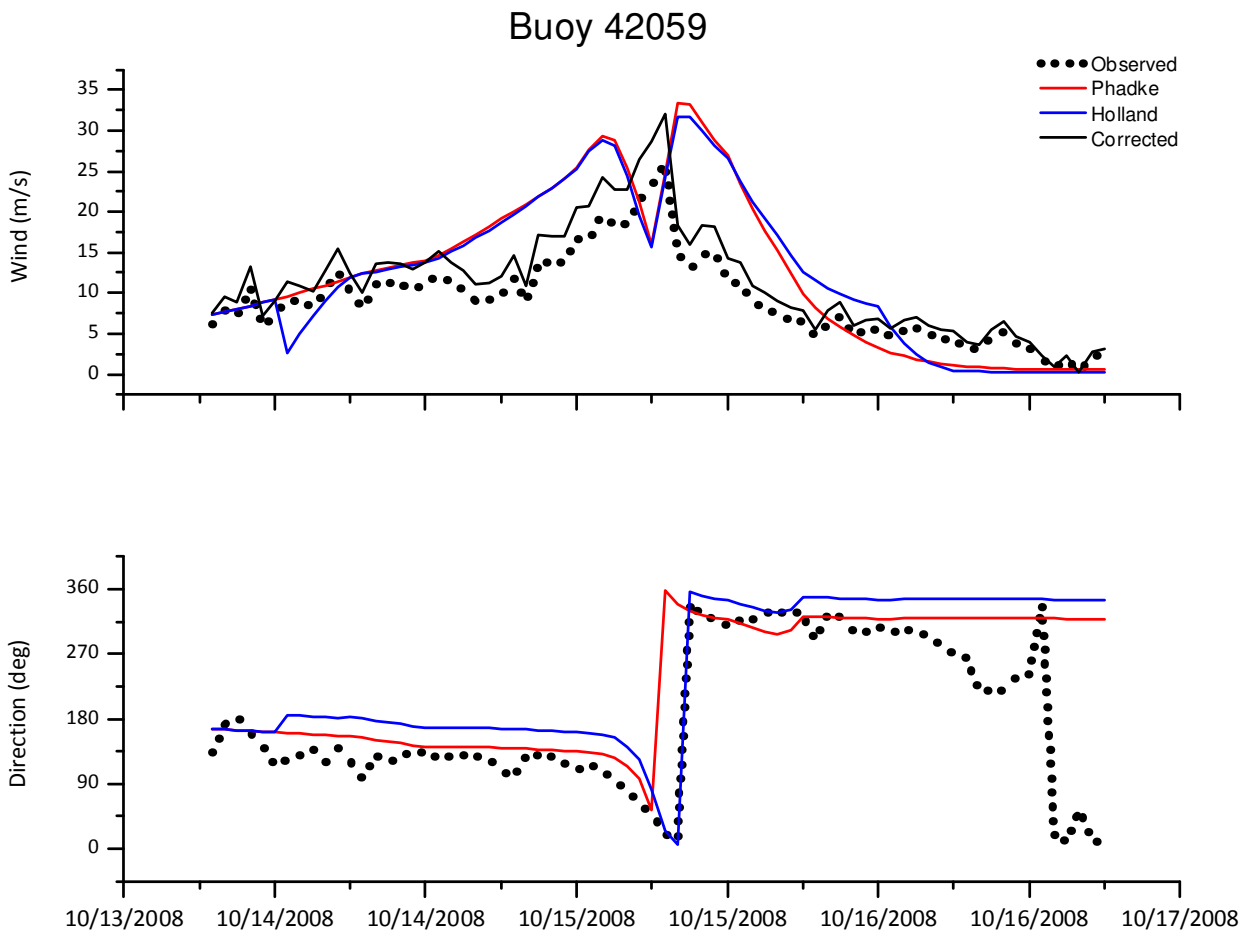

Figure 17. 10-meter wind speed (m/s) and direction (meteorological convention) during Hurricane Omar at buoy #42059. The observed wind speed represents the data measured by the instrument; the corrected wind speed represents the observed wind speed adjusted to marine exposure and 1-minute average.

parameter formulations only at NDBC Buoy 42059, where it is clear that the Holland (2008) formulation resembles the most the observed wind direction during the wind direction rotation due to the hurricane circulation. This is the most noticeable difference between the wind fields produced by the parametric wind model when changing the B parameter formulation. At NDBC Buoy 42059 and Charlotte Amalie the Holland (2008) formulation resulted in maximum winds that were closer to the adjusted wind observations, while for Christiansted Bay and Lime Tree Bay the Phadke, et al. (2003) formulation resulted in better maximum winds.

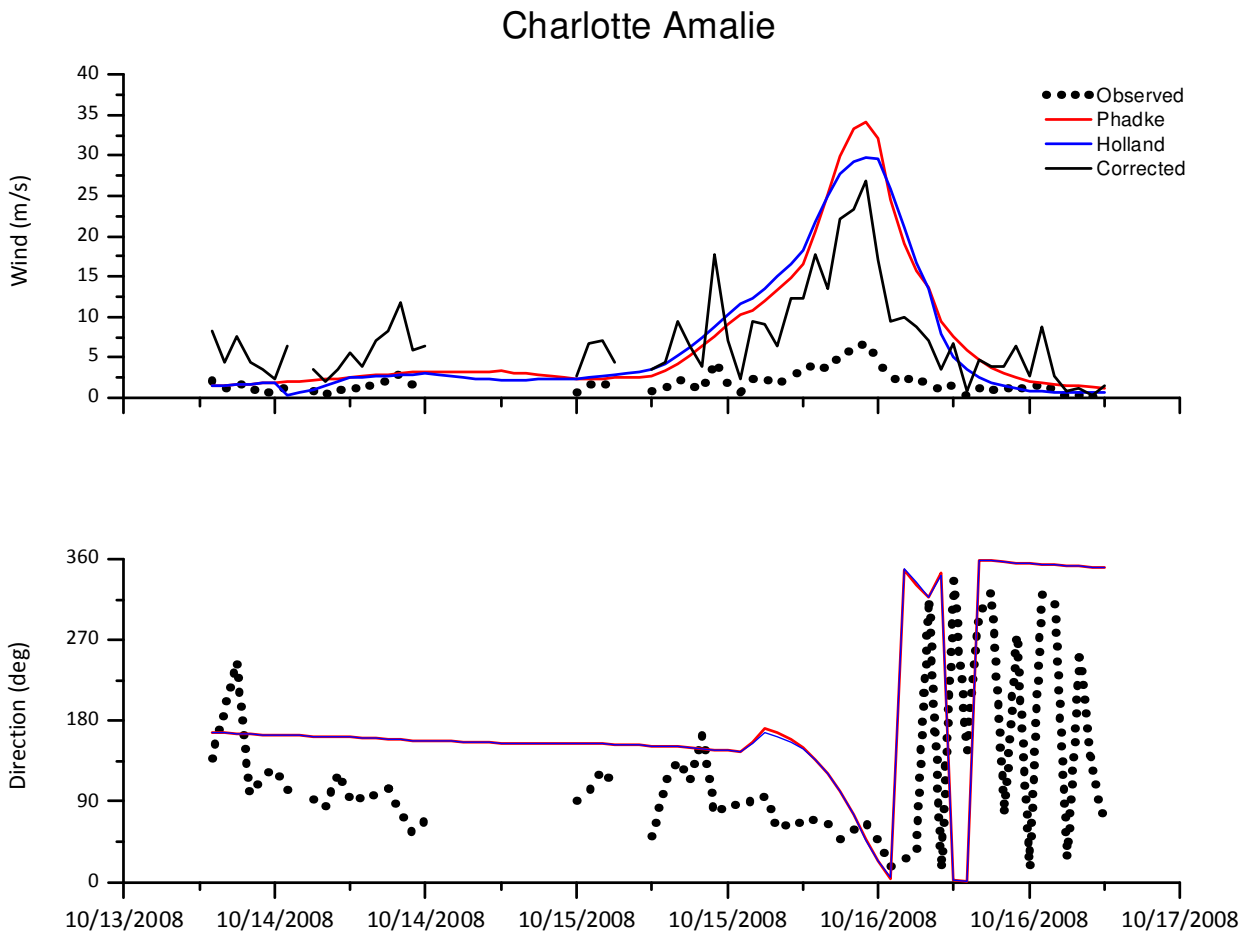

Figure 18. 10-meter wind speed (m/s) and direction (meteorological convention) during Hurricane Omar at Charlotte Amalie, VI. The observed wind speed represents the data measured by the instrument; the corrected wind speed represents the observed wind speed adjusted to marine exposure and 1-minute average.

As adjusting the observed winds affects only the magnitude of the winds and does not involve a directional correction (Westerink, et al. 2008), land influences on wind direction cannot be accounted for in the parametric model. Additionally, other variables that can influence the asymmetric wind distribution in the parametric model (Xie, Bao, et al. 2006), such as the inflow angle, are not included. These factors may account for the maximum wind peak time lag between the parametric and adjusted wind observations seen at NDBC Buoy 42059, Christiansted Bay, and Lime Tree Bay.

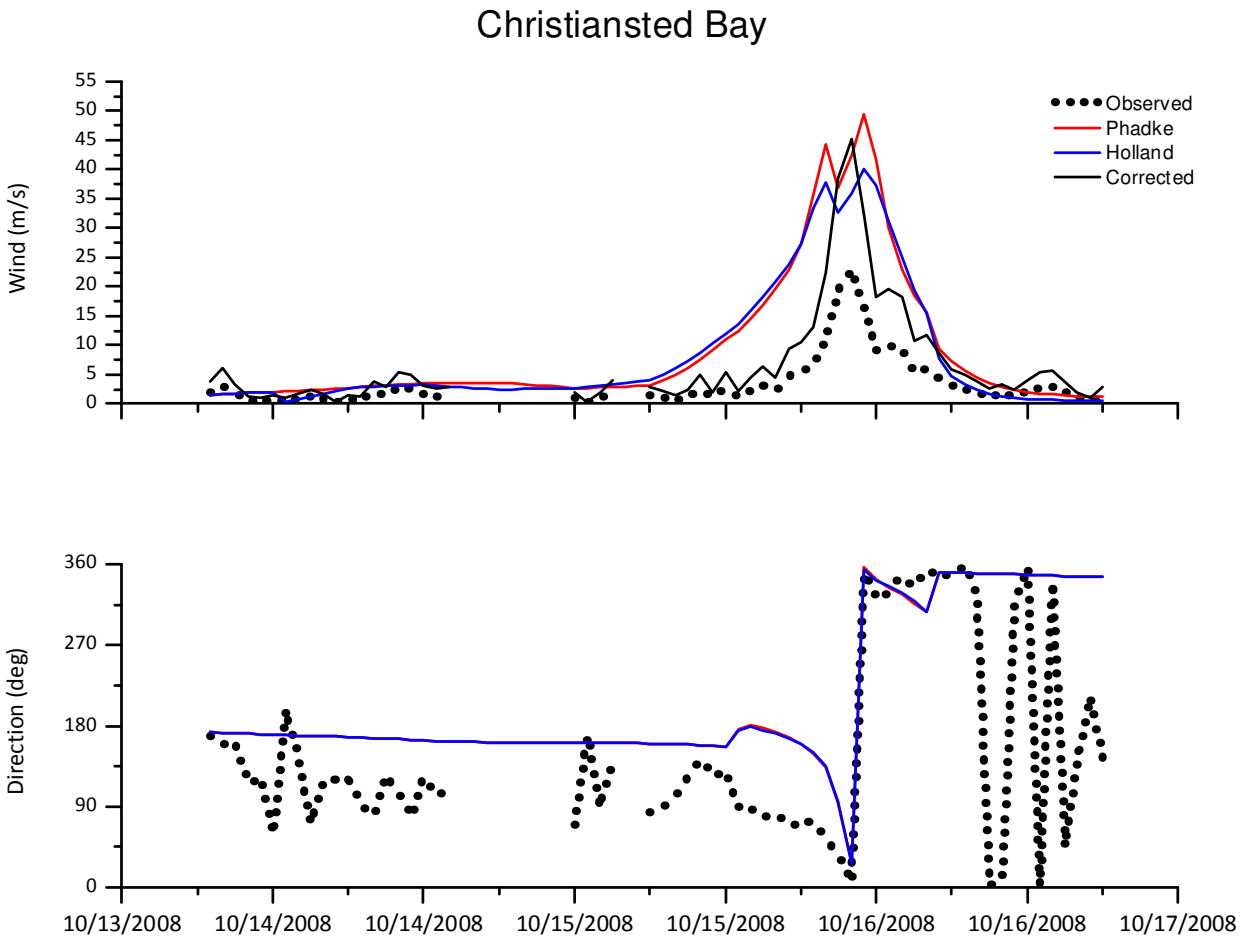

Figure 19. 10-meter wind speed (m/s) and direction (meteorological convention) during Hurricane Omar at Christiansted Bay, VI. The observed wind speed represents the data measured by the instrument; the corrected wind speed represents the observed wind speed adjusted to marine exposure and 1-minute average.

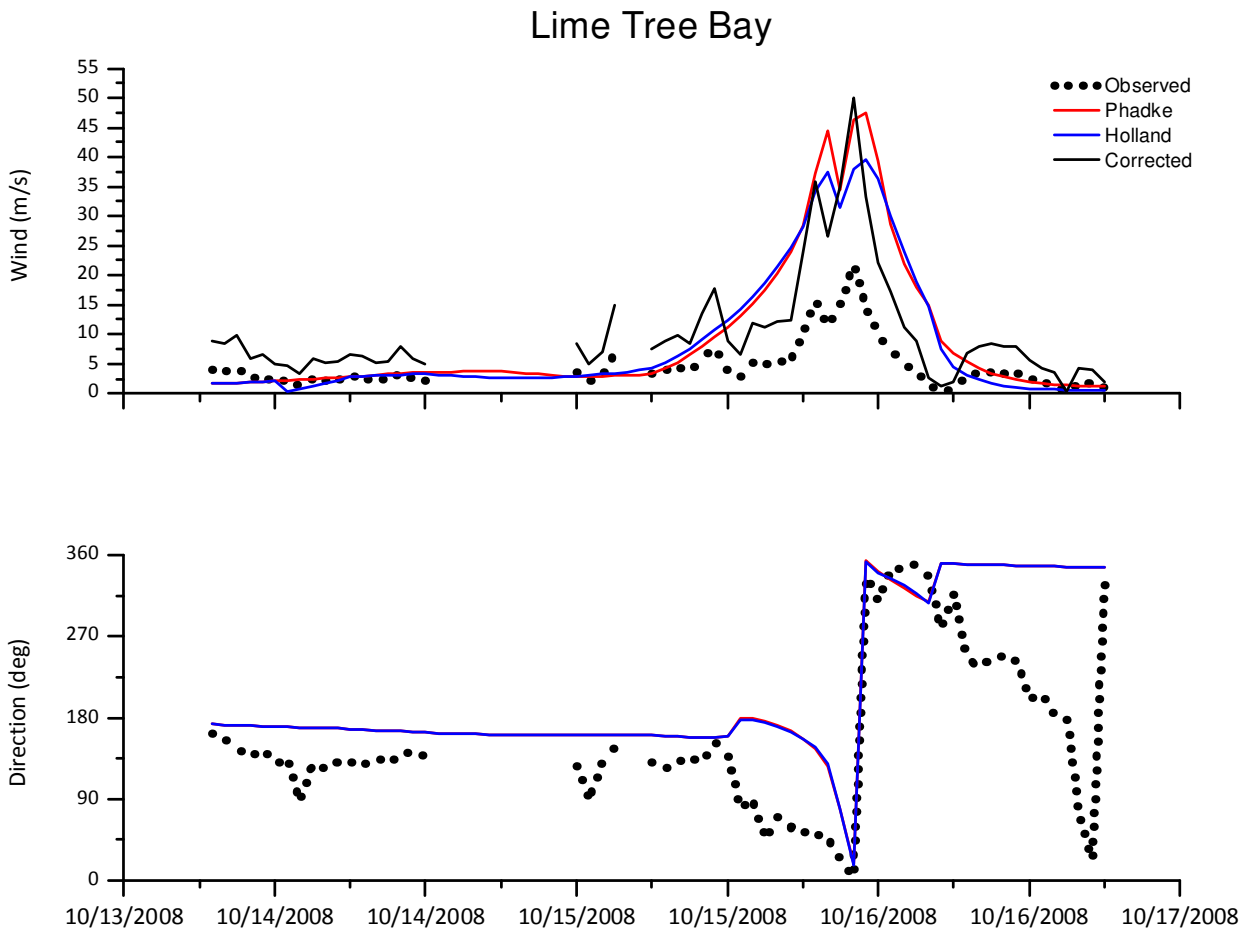

Figure 20. 10-meter wind speed (m/s) and direction (meteorological convention) during Hurricane Omar at Lime Tree Bay, VI. The observed wind speed represents the data measured by the instrument; the corrected wind speed represents the observed wind speed adjusted to marine exposure and 1-minute average.

4.3 Wave model results

The unSWAN wave model results were compared to buoy observations from both NOAAS's National Data Buoy Center (NDBC) buoy 42059 and buoy 41140. Model results could only be compared to buoy observations during Hurricane Omar since there were no buoys available during Hurricane Georges. The NDBC buoy 42059 was at a depth of 4.9 km and NDBC buoy 41140 was at a depth of 244 m. By using the wave dispersion relation on the observed maximum wave peak period it is determined that both buoys represent deep water wave conditions (I. R. Young 1999). Thus wave results from Hurricane Omar were used to validate waves at deep water and results from Hurricane Georges were used to examine the model behavior on coastal water waves, as Hurricane Georges track directly affected Puerto Rico.

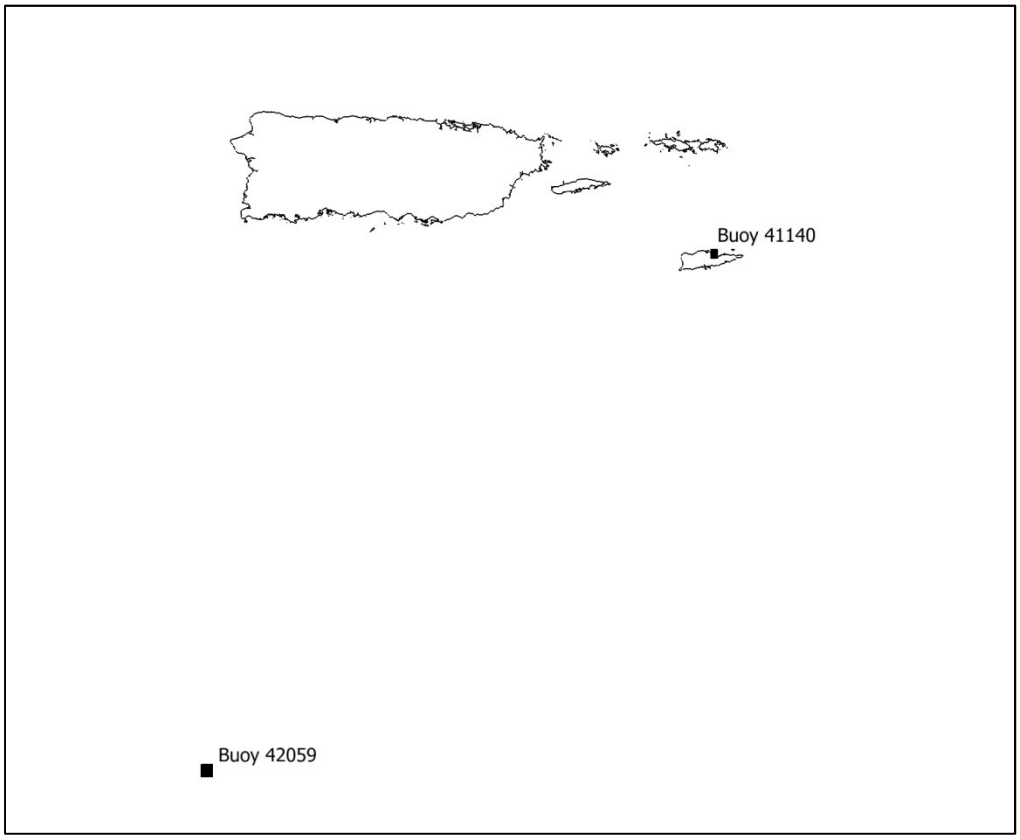

Figure 21. Location of NDBC buoy 42059 and NDBC buoy 41140.

The significant wave height, peak period and average period at the NDBC buoy 42059 during Hurricane Omar are shown in Figure 22. It can be seen that both the observed and modeled significant wave height follow the respective wind pattern (observed or modeled), with the modeled significant wave height being greater than the observed, as the modeled winds were higher. When refraction physics are allowed the peak period reaches the maximum period allowed in the model configuration, in this case 25 seconds. It is significant to notice that this peak period is reached during the time in which the area is not under the direct influence of the modeled hurricane winds and that the observed peak period does not exceeds 8 seconds during the time in which the peak period reaches 25 seconds in the model. In the case when refraction physics are not included in the model the peak period does not increases up to the maximum peak period allowed in the model.

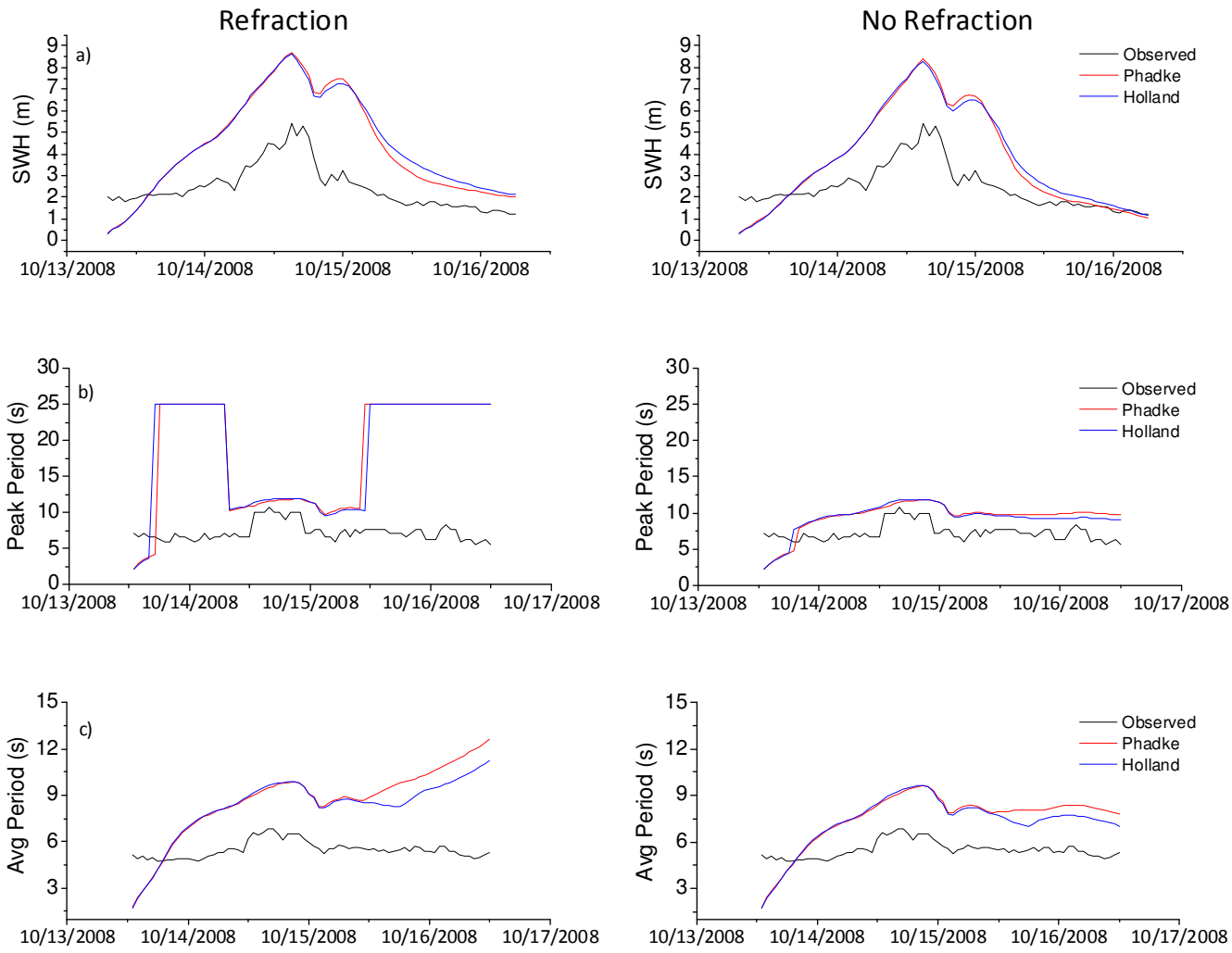

Figure 22. Significant wave height, peak period and average period during Hurricane Omar at NDBC Buoy 42059. Left panel shows results for the simulation including refraction in the unSWAN model and the right panel shows results for the simulation with no refraction in the unSWAN model. Black line represents observations, red line represents the results using the Phadke, et al. (2003) B-parameter formulation for the wind forcing and the blue line represents the Holland (2008) B-parameter formulation.

Results for the same variables at the NDBC buoy 41140 during Hurricane Omar are shown in Figure 23. As in the case of NDBC buoy 42059, both the observed and modeled significant wave heights follow both the observed and modeled wind patterns, and the modeled significant wave height was greater than the observed because of the modeled wind being higher. In contrast with the case of NDBC buoy 41140, the chosen B-parameter formulation causes a notable difference in the modeled significant wave heights. The peak period also reaches the maximum of 25 seconds when the area is not under the direct influence of the modeled hurricane winds. The observations show a peak period of about 15 seconds during the day prior to the hurricane winds influence, while the wind direction during this time indicate southerly winds of low intensity, which indicates that swell was arriving from the Atlantic Ocean and not the Caribbean Sea, as the location of the buoy relative to St. Croix, VI do not allow for possible swell created by the extended fetch (Moon, Ginis, et al. 2003, I. R. Young 2003) of Hurricane Omar to be measured. Figure 24 shows that the waves at the buoy were propagating from east during the studied period of time, indicating that the recorded swell had to be generated on the Atlantic Ocean.

The modeled significant wave height, peak period and average period at La Parguera, Puerto Rico during Hurricane Georges are shown in Figure 25. For this case the refraction has a marked effect on the significant wave height as the water is 3 meters deep. When refraction physics are included in the model the significant wave height stays almost constant during the model run, with a small increase when the highest hurricane winds reach La Parguera. It is

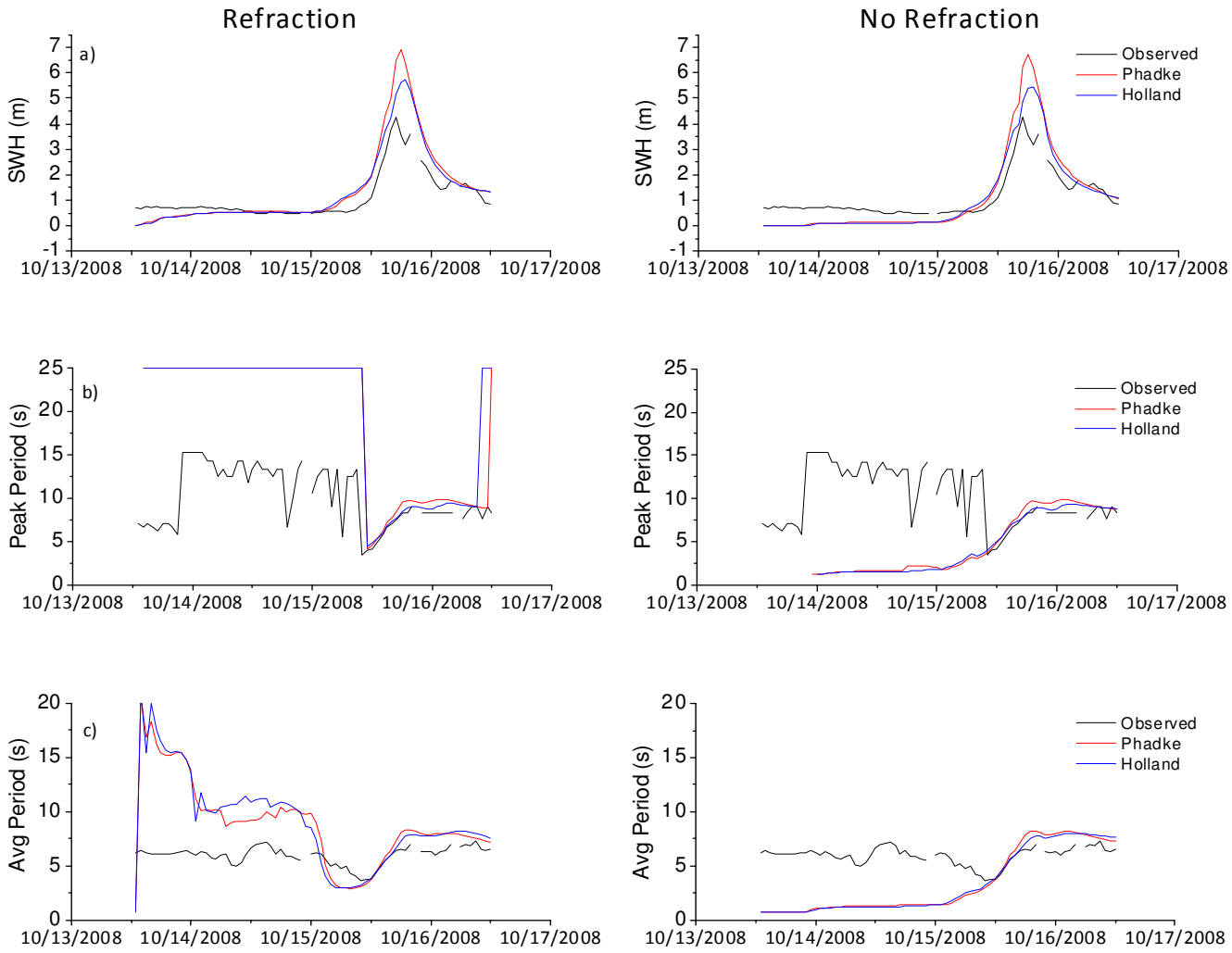

Figure 23. Significant wave height, peak period and average period during Hurricane Omar at NDBC Buoy 41140. Left panel shows results for the simulation including refraction in the unSWAN model and the right panel shows results for the simulation with no refraction in the unSWAN model. Black line represents observations, red line represents the results using the Phadke, et al. (2003) B-parameter formulation for the wind forcing and the blue line represents the Holland (2008) B-parameter formulation.

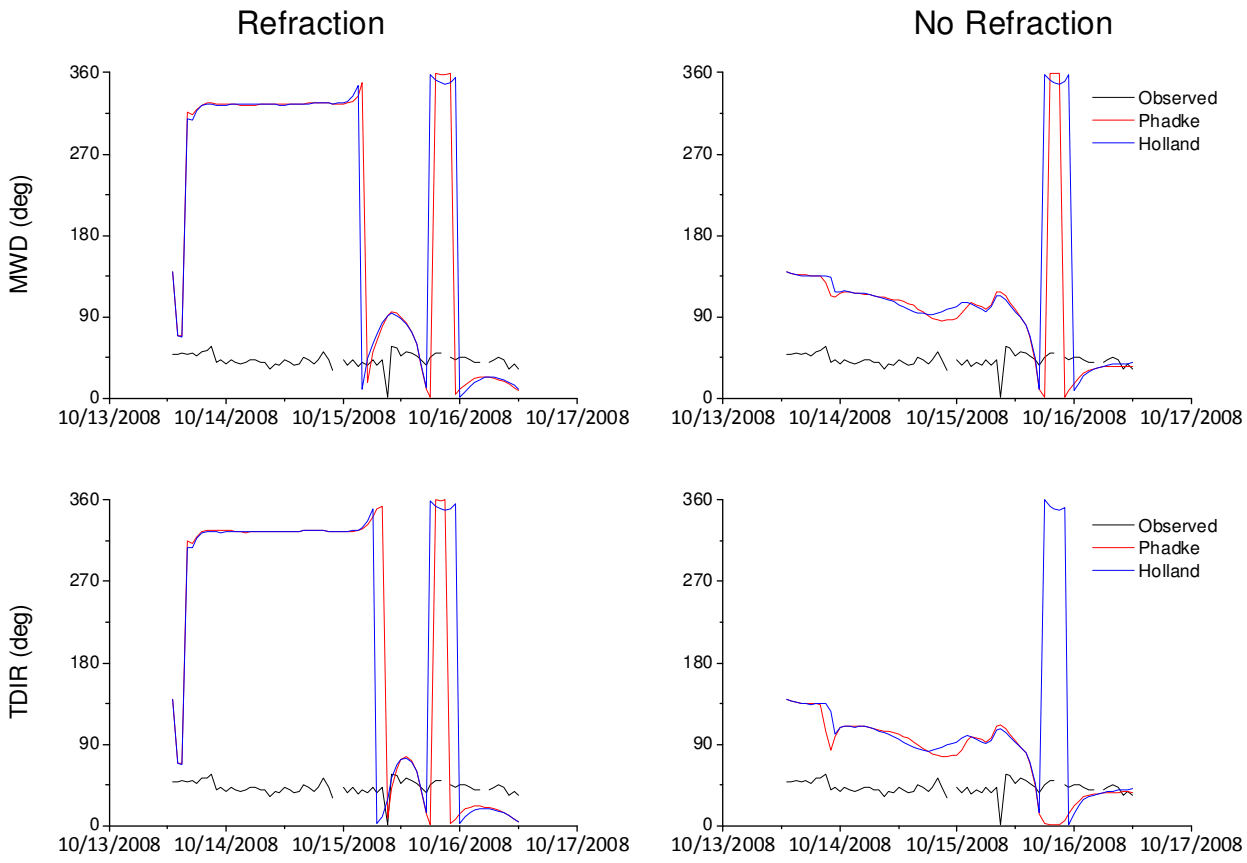

Figure 24. Mean wave direction and energy transport direction during Hurricane Omar at NDBC Buoy 41140. Left panel shows results for the simulation including refraction in the unSWAN model and the right panel shows results for the simulation with no refraction in the unSWAN model. Black line represents observations, red line represents the results using the Phadke, et al. (2003) B-parameter formulation for the wind forcing and the blue line represents the Holland (2008) B-parameter formulation.

clear that the significant wave height does not increase as the wind speed increases. If refraction is not taken into account in the wave model then the significant wave height increase as the wind speed increases, following the same pattern observed and modeled in the deep water cases during Hurricane Omar. The peak period also reaches the maximum 25 seconds when refraction is included in the model, but contrary to what is seen on deep water, in La Parguera the peak period stays at the maximum even when the area is under the direct

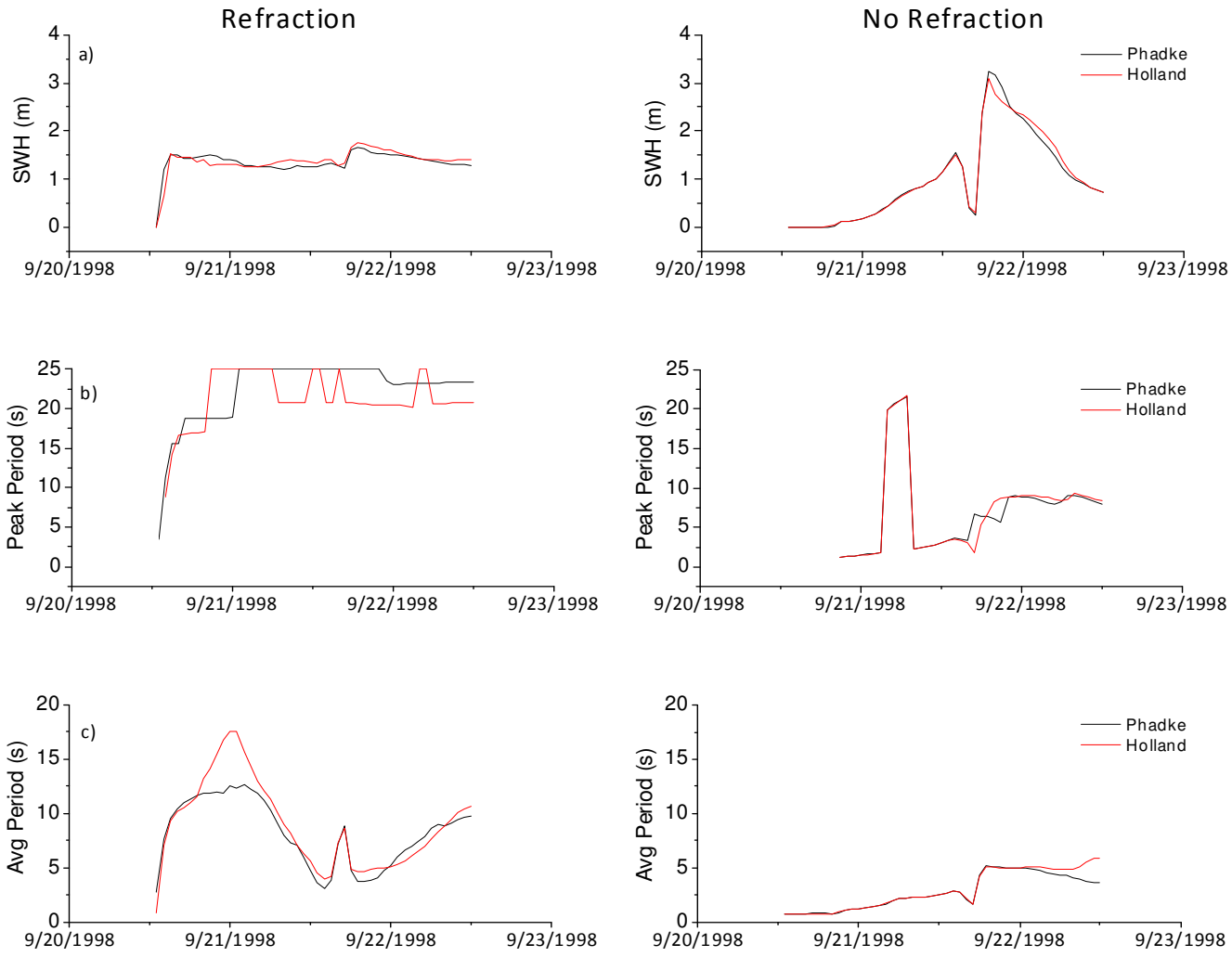

Figure 25. Significant wave height, peak period and average period during Hurricane Georges at La Parguera, Puerto Rico. Left panel shows results for the simulation including refraction in the unSWAN model and the right panel shows results for the simulation with no refraction in the unSWAN model. Red line represents the results using the Phadke, et al. (2003) B-parameter formulation for the wind forcing and the blue line represents the Holland (2008) B-parameter formulation.

influence of the modeled hurricane winds. Even though during short spaces of time the peak period does not stay at the maximum allowed period this do not correspond directly to the hurricane wind influence in the area, and the lack of observed wave records makes it inconclusive to decide on a relationship between winds and peak periods for this case. Figure 26 shows the mean wave direction and energy transport direction at La Parguera during Hurricane Georges. The refraction causes the waves to propagate towards the coast, while when no refraction is included the waves propagate in

the direction of the wind. The effects of wave-current interaction are seen in the differences between the mean wave direction and the energy transport direction, which accounts for the effect of current direction.

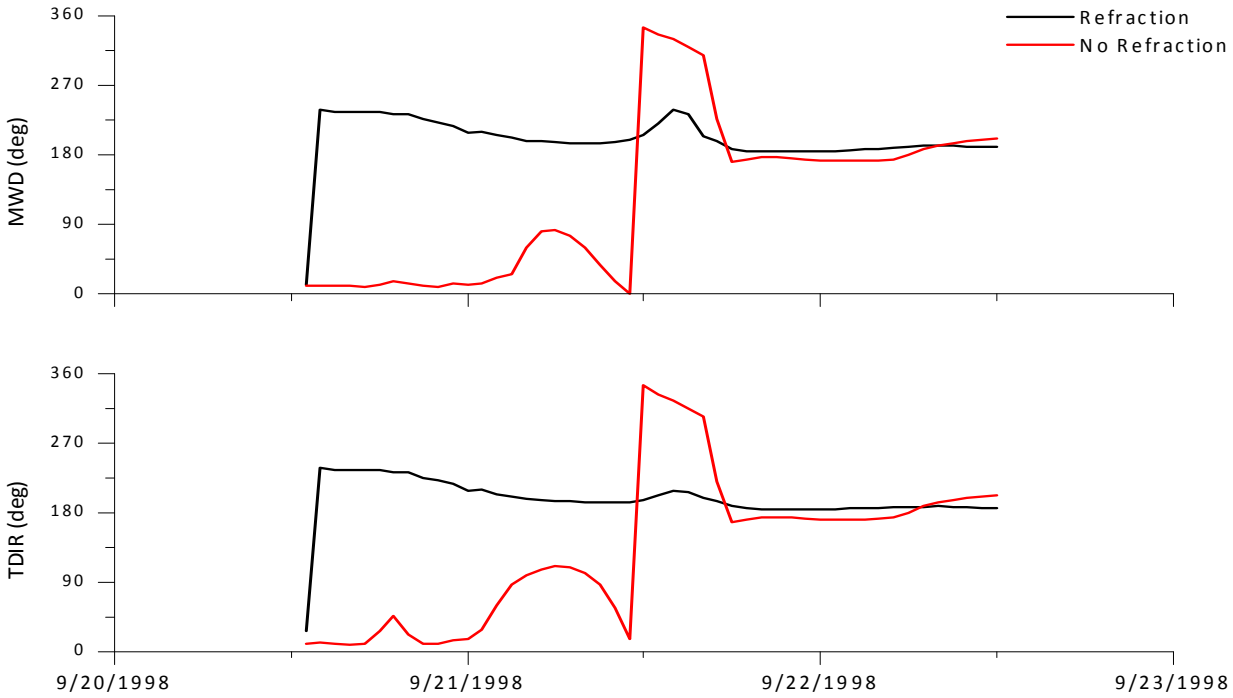

Figure 26. Mean wave direction and mean energy transport direction during Hurricane Georges at La Parguera, Puerto Rico. In this case the parametric wind model used the Holland (2008) B-parameter formulation. Black line represents the simulation with refraction and red line represents the simulation with no refraction.

The energy dissipation caused by depth-limited wave breaking and white-capping explains the stabilizing effect of refraction on the significant wave height. Figure 27 shows the energy dissipation and the breaker fraction at La Parguera during Hurricane Georges. It can be seen that when refraction is included in the model the energy dissipated by depth-limited wave breaking is much greater than the energy dissipated when no refraction is included in the model during the time before the direct influence of hurricane winds in the area. As the wind reaches the local maximum wind speed the

depth-limited wave breaking energy dissipation reaches a peak in both cases, with the dissipation of energy when no refraction is included rising sharply and being greater during this wind speed peak. After this wind speed peak the energy dissipation in the no refraction case diminishes and the dissipation in the simulation including refraction is greater again. Moreover, the breaker fraction is always greater when refraction is included in the model, as is the energy dissipation due to white-capping. These three processes behave as it would be expected under the influence of refraction, with the wave's wavelength decreasing as it propagates towards shallower water causing the wave steepness to increase and in turn cause more wave-breaking action and energy dissipation (I. R. Young 1999, Holthuijsen 2007). These factors cause the significant wave height to be capped under the effect of refraction as it is clearly shown in the model results.

Difference statistics during Hurricane Omar for significant wave height, average period, peak period and wave direction are shown in Table 9, Table 10,

Table 11 and Table 12 respectively. The mean absolute error (MAE) and root mean squared error (RMSE) are as defined previously, and the Willmott index of agreement is defined as (Willmott 1982) which is a measure of model/observations agreement:

$$d = 1 - \left[\frac{\sum_{i=1}^{N}(P_i - O_i)^2}{\sum_{i=1}^{N}(|P'_i| + |O'_i|)^2}\right]$$

where P_i are the model results and O_i are the observations and $P'_i = P_i - \overline{O}_i$ and $O'_i = O_i - \overline{O}_i$.

As the observed wave records show, the significant wave height, peak period and average period prior to the direct influence of the hurricane winds on each location were not affected by an extended fetch

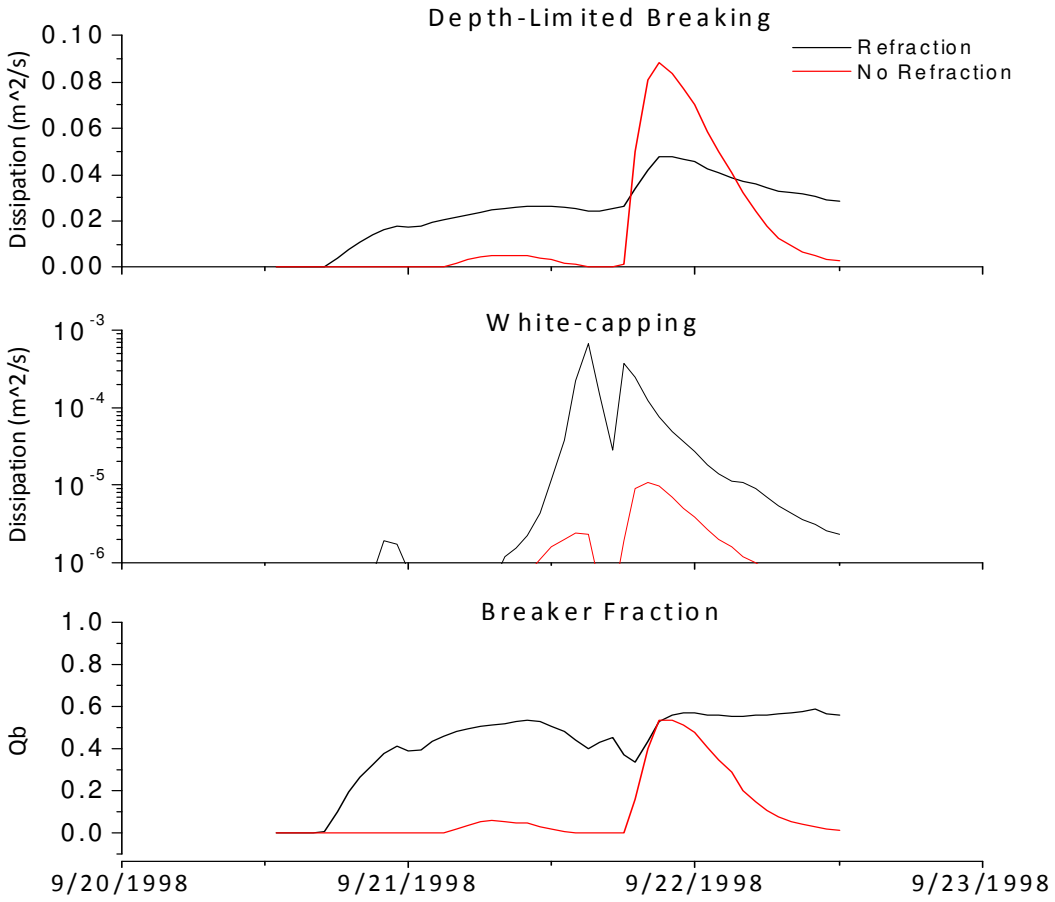

Figure 27. Energy dissipation caused by depth-limited breaking and white-capping, and fraction of waves breaking during Hurricane Georges at La Parguera, Puerto Rico. Results from the unSWAN model with and without refraction processes (black and red lines, respectively).

effect caused by Hurricane Omar. Additionally, unSWAN was not being able to include a prior sea state as no wave spectrum is used as either initial or boundary conditions, so these statistics are calculated only for the period of time in which each location is under the direct influence of the modeled hurricane winds.

The statistics for significant wave height show that for all cases it was overestimated and that the B-parameter formulation that produced the lowest MAE and RMSE was Holland (2008). The average periods were overestimated in all cases, but in NDBC buoy 41140 the RMSE ranged from 0.9483 to 1.1345 compared to NDBC 42059 where it ranged from 2.6410 to 3.0445. The peak periods

show similar difference statistics, with the SWAN model doing better at NDBC buoy 41140 with RMSE ranging from 0.9483 to 1.1345.

Table 9. Difference statistics for significant wave height at NDBC Buoys 42059 and 41140 during Hurricane Omar.

	Significant Wave Height			
	Phadke		Holland	
	Refraction	No Refraction	Refraction	No Refraction
	NDBC Buoy 42059			
MAE	3.4655	2.9021	3.4161	2.8554
RMSE	3.5327	2.9733	3.4784	2.9182
Wilmott Index	0.37	0.4323	0.3738	0.4377
	NDBC Buoy 41140			
MAE	1.0201	0.9073	0.7466	0.6294
RMSE	1.3619	1.2489	0.9799	0.8433
Wilmott Index	0.7592	0.7859	0.8299	0.8631

Table 10. Difference statistics for average period at NDBC Buoys 42059 and 41140 during Hurricane Omar.

	Average Period			
	Phadke		Holland	
	Refraction	No Refraction	Refraction	No Refraction
	NDBC Buoy 42059			
MAE	3.0304	2.6232	3.0304	2.6201
RMSE	3.0445	2.646	3.0418	2.641
Wilmott Index	0.2555	0.2927	0.2606	0.2997
	NDBC Buoy 41140			
MAE	0.8511	0.8847	0.7538	0.7039
RMSE	1.098	1.1345	0.9949	0.9483
Wilmott Index	0.8052	0.7919	0.8346	0.8384

Table 11. Difference statistics for peak period at NDBC Buoys 42059 and 41140 during Hurricane Omar.

	Peak Period			
	Phadke		Holland	
	Refraction	No Refraction	Refraction	No Refraction
	NDBC Buoy 42059			
MAE	2.8872	2.6225	2.8919	2.6638
RMSE	3.0907	2.8269	3.0629	2.8382
Wilmott Index	0.5047	0.5409	0.5231	0.5547
	NDBC Buoy 41140			
MAE	0.9266	0.9549	0.5015	0.55
RMSE	1.0678	1.0665	0.6399	0.6705
Wilmott Index	0.9013	0.8963	0.9566	0.9498

Table 12. Difference statistics for mean wave direction and energy transport direction at NDBC buoy 41140 during Hurricane Omar.

	Phadke		Holland	
	Refraction	No Refraction	Refraction	No Refraction
	Mean Wave Direction			
MAE	29.6509	26.373	32.0617	30.3086
RMSE	32.3006	31.4554	35.6252	34.0595
	Energy transport direction			
MAE	26.5664	23.7908	28.7443	26.6442
RMSE	29.3103	29.0198	34.6959	32.7033

It should be noted that when the observed and modeled data set is limited to the period of time under direct influence of the hurricane winds the maximum peak period of 25 seconds is absent. Figure 28 shows the distribution of the modeled wind speed when the peak period is the maximum of 25 seconds. The maximum peak period is reached only when the wind speed is under 20 m/s, which falls under the lowest limit for a Category 1 under the Saffir-Simpson scale. The maximum occurrence of the maximum peak period is when the wind speed is 3 m/s. This will be further analyzed in the discussion section.

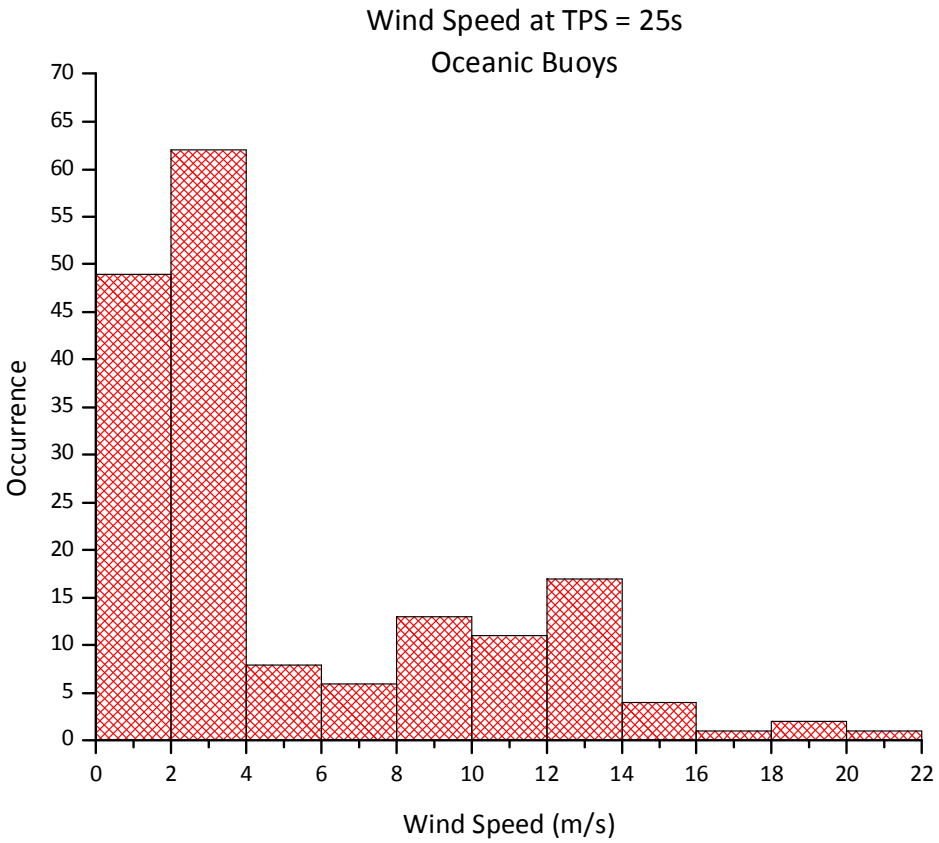

Figure 28. Distribution of modeled wind speeds during the wave peak periods of 25 seconds during Hurricane Omar at NDBC Buoys 42059 and 41140.

4.4 Water Level

To validate the overall model performance, the water level was studied during Hurricane Georges. As we are interested in the effects of meteorological and wind-driven forcing, we focus on the prediction of the residual (de-tided) surface elevation. For the case of observations this residual surface elevation is the observed water level record minus the harmonically predicted water level and for the simulated residual surface elevation the total modeled water level minus the modeled tidal prediction (Brown and Wolf 2009). Additionally, the residual surface elevation caused by wind setup and wave setup were calculated to show their respective influence on the water level. The hurricane wind field was calculated using the previously studied B-parameter formulations (Phadke, et al. 2003, Holland 2008). Only water level records and simulations for Hurricane Georges were taken into consideration as this has been the strongest hurricane to directly affect Puerto Rico in the recent history, providing a strong enough meteorological forcing in our coasts (Landsea 2010).

Table 13. Difference statistics at San Juan tide gauge during Hurricane Georges.

	Observed	**Wind Setup**		**Wind and Wave Setup (refraction)**		**Wind and Wave Setup (no refraction)**	
		Phadke	Holland	Phadke	Holland	Phadke	Holland
Mean	0.0398	0.0146	0.0135	0.0563	0.0530	0.0702	0.0690
Max	0.4800	0.2473	0.2473	0.5306	0.5292	0.6502	0.6506
MAE	-	0.1014	0.0986	0.1116	0.1078	0.1183	0.1142
RMSE	-	0.1276	0.1238	0.1277	0.1240	0.1425	0.1379
Willmott Index	-	0.6720	0.6916	0.7991	0.8100	0.7920	0.8039

Two locations at Puerto Rico were used to validate the water level during Hurricane Georges: San Juan and La Parguera. These were the only locations on which water level records were available. Both tide gauges were operated by NOAA's National Ocean Service. The previously defined difference statistics were used to quantify the model accuracy: maximum absolute error (MAE), root mean square error (RMSE) and Willmott's index of agreement (Willmott 1982).

Figure 29 shows the residual surface elevation at the San Juan tide gauge during Hurricane Georges and Table 13 the difference statistics. There is a noticeable difference between the residual elevation caused only by wind setup and that caused by both wind and wave setup. When both wind and wave setup are considered the maximum residual elevation ranges from 0.53 to 0.53 m and 0.65 to 0.65 m for simulations with and without refraction physics respectively, while the maximum residual elevation when only wind setup is considered is 0.25 m. The observed maximum residual elevation was 0.4800 m. At this location there is an evident time discrepancy between the modeled and observed peak residual surface elevation, which resembles the time discrepancy between the modeled and observed peak wind speed. This time discrepancy has been found on previous studies (Xie, Bao, et al. 2006) and can be attributed to be an effect of the parameterization of the hurricane. The parametric model uses a symmetric radius of maximum wind, whereas an asymmetric radius of maximum wind would cause that the winds at a particular location arrive earlier or later, depending on the radius of maximum winds at that particular wind field quadrant.

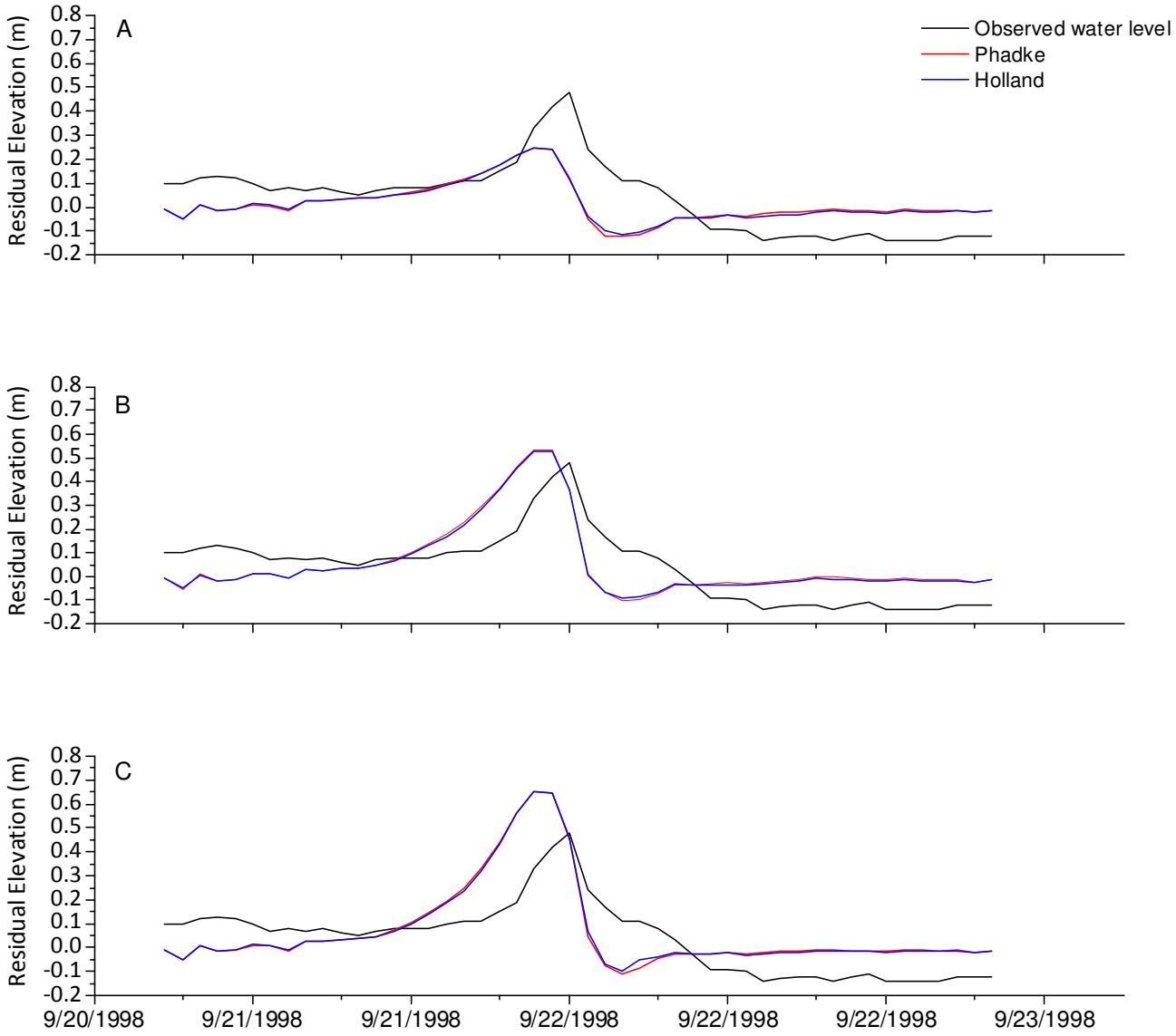

Figure 29. Residual surface elevation during Hurricane Georges at San Juan, Puerto Rico. A) Observed water level and modeled wind setup forced with tides, pressure and wind fields, no wave coupling. B) Observed water level and modeled wind and wave setup: model forced with tides, pressure, wind fields and full water level-currents-waves coupling with refraction physics. C) Observed water level and modeled wind and wave setup: model forced with tides, pressure, wind fields and full water level-currents-waves coupling with no refraction physics.

Results for the residual surface elevation at La Parguera are shown on Figure 30 and difference statistics are shown on Table 14. Contrary to the case of San Juan, in La Parguera there is not a great influence of the wave setup on the residual surface elevation. This can be seen on Figure 31, with the wave setup on San Juan ranging from 0.3 to 0.45 m while in La Parguera it ranged from -0.05 to 0.15 m. It is worth noting that in La Parguera, the maximum residual elevation that better simulated the observed maximum was in the case when only wind setup was taken into account in the model. This case also had the best index of agreement with a value of 0.8325 and 0.8462 for each B-parameter formulation.

Table 14. Difference statistics at La Parguera tide gauge during Hurricane Georges.

	Observed	Wind Setup		Wind and Wave Setup		Wind and Wave Setup (no refraction)		Loosely Coupled 30-m resolution
		Phadke	Holland	Phadke	Holland	Phadke	Holland	Holland
Mean	0.1238	0.0938	0.0956	0.1313	0.1837	0.1254	0.1256	0.0956
Max	0.6000	0.7951	0.7300	0.8548	0.8226	0.8158	0.7399	0.7300
MAE	-	0.1004	0.0965	0.1242	0.1008	0.1085	0.1063	0.1015
RMSE	-	0.1340	0.1240	0.1776	0.1519	0.1574	0.1449	0.1291
Willmott Index	-	0.8325	0.8462	0.7557	0.7969	0.7914	0.8078	0.8366

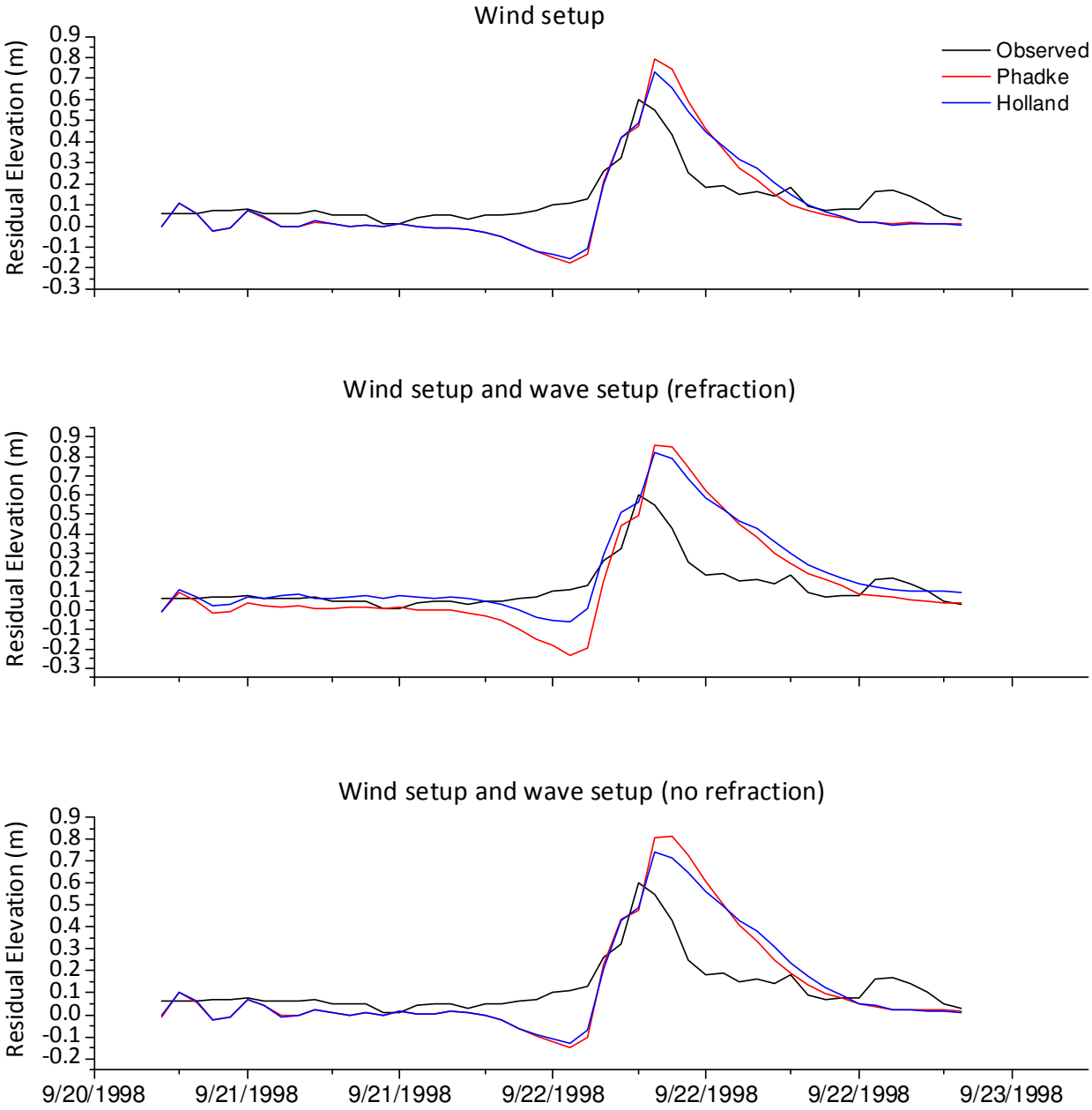

Figure 30. Residual surface elevation during Hurricane Georges at La Parguera, Puerto Rico. Wind setup: model forced with tides, pressure and wind fields, no wave coupling. Wind setup and wave setup (refraction): model forced with tides, pressure, wind fields and full water level-currents-waves coupling with refraction physics. Wind setup and wave setup (no refraction): model forced with tides, pressure, wind fields and full water level-currents-waves coupling with no refraction physics

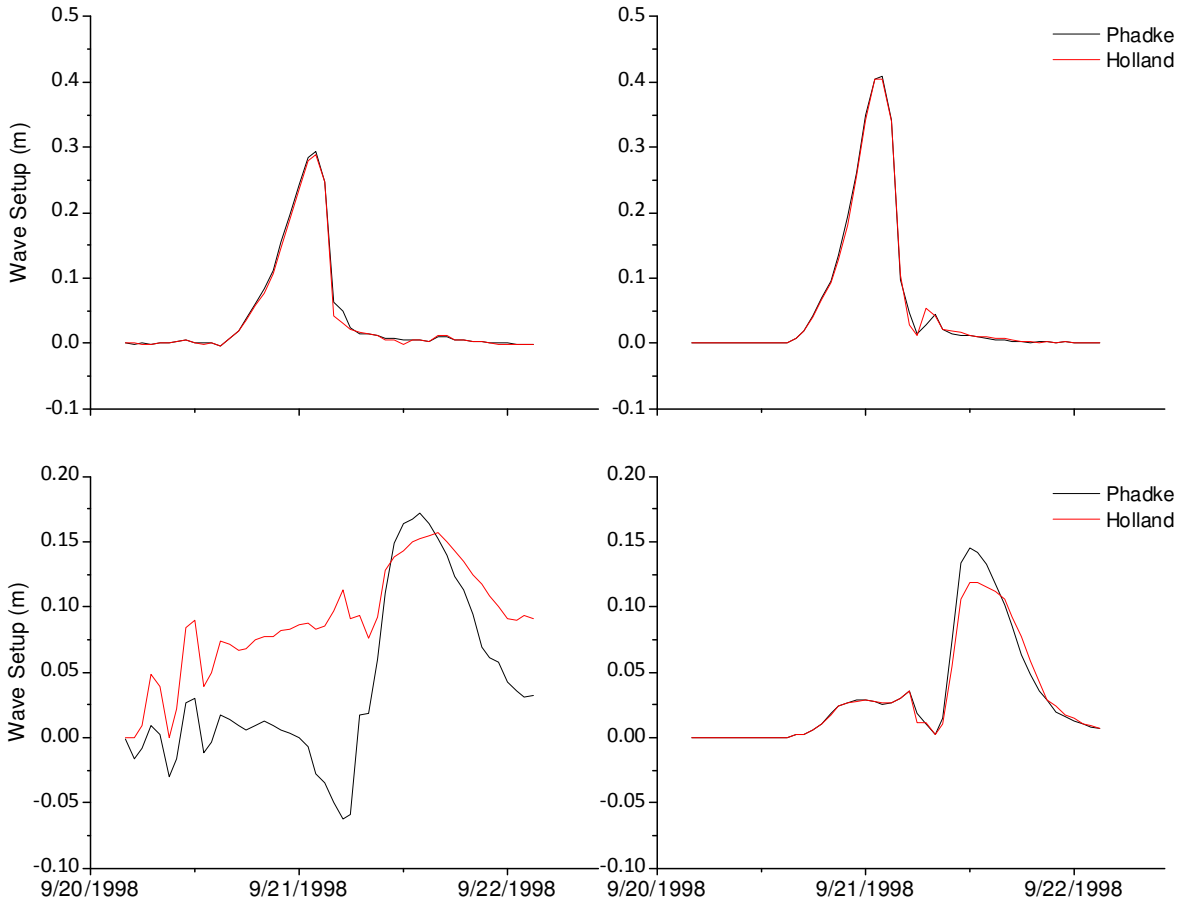

Figure 31. Wave setup at San Juan (upper panel) and La Paguera (lower panel) during Hurricane Georges. The left column represents the simulation for the fully coupled model with refraction physics and the right column represents the simulation for the fully coupled model with no refraction physics.

Simulating the Hurricane Georges storm surge using ADCIRC+SWAN resulted in both a lower residual surface elevation and wave setup. For this simulation the wave radiation stresses were computed on a SWAN structured mesh with a resolution of 30 meters. At such a high resolution all reefs and abrupt bathymetry are properly represented in the computational domain, while the unstructured grid used in the ADCIRC+unSWAN model does not represent these bathymetric features at such detail. The upper panel on Figure 32 shows that the residual surface elevation from ADCIRC+SWAN was lower in magnitude and had a shorter time span than the resulting surface

elevation from ADCIRC+unSWAN . The wave setup from ADCIRC+SWAN is also lower than the wave setup ADCIRC+unSWAN, and the difference statistics on Table 14 show that the index of agreement for ADCIRC+SWAN is almost equal to that of the water level when only wind setup was considered in the model.

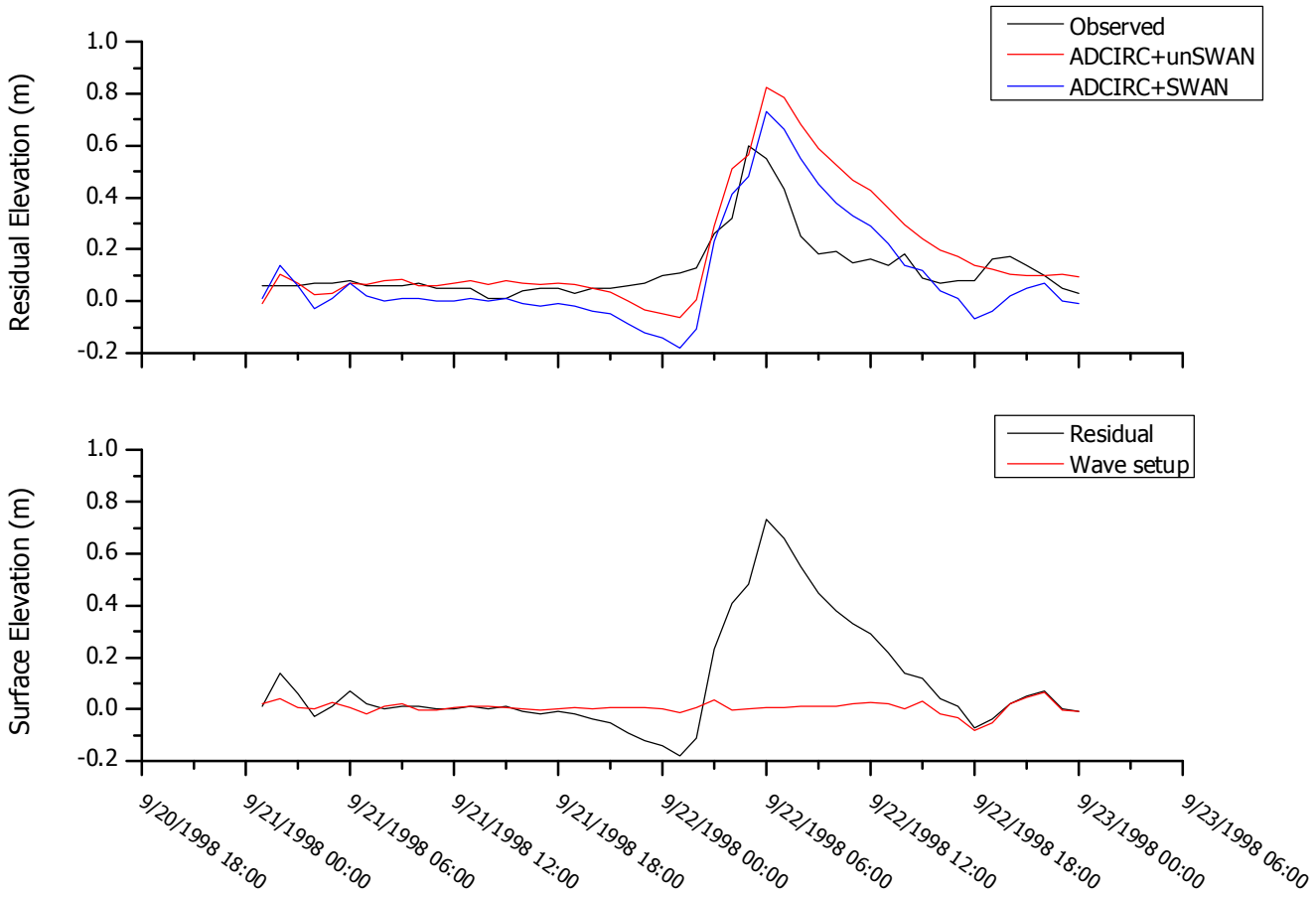

Figure 32. Upper panel: Observed and modeled residual surface elevation during Hurricane Georges at La Parguera, Puerto Rico. Lower panel: Residual surface elevation and wave setup from the ADCIRC+SWAN.

This decrease in both residual surface elevation and wave setup for the ADCIRC+SWAN can be explained by the increase in bathymetric features that are represented in the computational domain when a high resolution mesh is used to calculate the wave-induced radiation stresses. The wave setup is caused by horizontal variations in the in the radiation stress (Holthuijsen 2007), which in turn has a quadratic dependence on wave amplitude. As the waves break on shallow waters, the wave amplitude diminishes towards the coast and so the radiation stress also diminishes, but the wave-induced force has a negative relationship with the horizontal gradient of radiation stress, thus creating a positive force towards the shore. This in turn creates a positive water level slope towards the shore and a subsequent wave setup. In ADCIRC+unSWAN the reefs and bathymetric features are under-resolved due to the grid resolution, and so the sheltering effect of these features is diminished. Henceforth, more wave energy is dissipated in the near shore, where the La Parguera tide gauge lies, producing there larger radiation stress gradients. In contrast, when the bathymetry is properly resolved in the higher resolution regular mesh, the sheltering effect of the reefs results in a decrease of wave energy reaching the near shore, and a subsequent smaller wave setup.

5 Discussion

5.1 Parametric wind model

Both B-parameter formulations resulted in distinct hurricane wind fields. For each hurricane, the resulting wind field had different spatial wind distributions and different maximum wind speeds. These differences were determined by the B-parameter resulting from each formulation, as this parameter defines the wind field shape and all the other variables in the parametric wind model were held constant for each hurricane. There is no clear pattern regarding as to if the B-parameter will be greater for either of the formulations for any given case. That is, from the results it cannot be determined if either B-parameter formulation will always be greater than the other. In addition, the hurricane's wind asymmetry imparted by the hurricane's translation speed causes the wind profile's shape to change depending on the respective hurricane's quadrant, so the wind distribution will not be symmetric as it would on the original Holland (1980) model. This causes the wind profile at a given location to depend on its position relative to the hurricane's center and so the B-parameter would not be the only factor to determine the profile shape at a given position. Nevertheless the results show that for all cases the Phadke, et al. (2003) formulation resulted in higher maximum winds.

The lack of a surface roughness length parameterization on the model greatly affects the correct modeling of the wind field as the hurricane interacts with land. By adjusting the observed winds to a corresponding marine exposure it was shown that the parametric wind model was in good agreement with these equivalent winds at a marine exposure. This indicates that in order to fully describe the winds at the coast as the hurricane approaches land, a roughness length parameterization is needed to be added into the mesh. Recent studies have described methods to implement this capability based on land cover data (Westerink, et al. 2008).

As the coupled model configuration is such that winds are passed from ADCIRC to SWAN, if a

roughness length parameterization were to be included in the mesh, there may be a need to take into consideration the effects that the wave field has on the effective roughness length over the ocean on both models. It has been found that the wave age (cp/u*; cp = phase speed at peak frequency, u* = wind friction velocity) has an influence on the effective roughness length over the ocean by means of the Charnock parameter (Moon, Hara and Ginis 2004, Moon, Ginis and Hara 2004, Brown and Wolf 2009), and experiments for tropical cyclones indicate that for growing young seas and high winds a constant Charnock parameter may lead to an overestimation of the momentum exchange across the air-sea interface (Moon, Ginis and Hara 2004). Possible evidence of this phenomenon is seen on Figure 22, where the significant wave height was overestimated with a mean absolute error of up to 3.46 m while the wind speed was also overestimated even when this location was on deep water, away from the coast, and so the parametric model should have had a better performance. An effective roughness length dependent on the local wave field state would have resulted on a lower wind stress and significant wave height at this location. Moreover, if this effective roughness length were to be coupled back into the ADCIRC model it would have implications for the circulation results as well, especially on the shallow waters where the wind stress has a greater importance on the momentum equation (Westerink, et al. 2008).

It must be noted that the default wind drag coefficient formulation which was used for SWAN ans unSWAN is not based on a Charnock parameter and so does not provide an effective roughness length to be used on both coupled models. The formulation has a linear relationship between the drag coefficient and the wind speed. This linear behavior furthers the overestimation of the drag coefficient as found on previous studies (Moon, Hara and Ginis 2004, Moon, Ginis and Hara 2004), which indicate that the wind drag coefficient behavior is not linear for all wind speeds and sea states. Specifically, the wind drag coefficient formulation used on the SWAN model has been found to greatly

overestimate the drag coefficient at speeds over 30 m/s when compared to a coupled wind-wave boundary layer formulation. The effect of wind stress parameterization on surface water levels will be further discussed on the water level discussion.

5.2 unSWAN model

The validation results show that the model performed better at the NDBC Buoy 41140 than at NDBC Buoy 42059. Significant wave height was overestimated for both locations with a maximum MAE of 1.02 m and 3.47 m and RMSE of 1.36 m and 3.53 m, respectively. The Willmott's (1982) index of agreement clearly shows that the model simulated the significant wave height much better at NDBC Buoy 41140 with a maximum index of 0.86 while the maximum at NDBC Buoy 42059 was only 0.44. The parameter which was better represented by the model at both locations was the peak period with a maximum index of agreement of 0.9566 for NDBC Buoy 41140 and 0.5547 for NDBC Buoy 42059. Even when this was the parameter in which the model had the better performance for both locations, the NDBC Buoy 41140 had much better results as demonstrated by the index of agreement and a minimum MAE of 0.5015 s.

Such a discrepancy in the performance of the model for these two locations could be explained by the difference on the spatial resolution of the computational mesh between these two locations. Although both locations represent deep-water wave conditions based on the d/L (d=water depth, L=wavelength) rule (I. R. Young 1999), the resolution on the area near NDBC Buoy 42059 is about 60 km and near NDBC 41140 is about 200 meters. Thus the model had a better performance at the location with the highest resolution. This is consistent with results of previous studies with surge-wave models (Bunya, et al. 2010), in which a resolution of about 5.5 km has been used for offshore waters such as NDBC Buoy 42059 and about 200 m for near shore locations such as NDBC 41140.

Comparing our mesh resolution to the one just cited, it is clear that our resolution near NDBC Buoy 42059 is too coarse, thus leading to solution errors. A similar sensitivity to spatial resolution was found on a study which used the same ADCIRC+unSWAN coupled model as the present study (Dietrich, Bunya, et al. 2010) (Dietrich, Bunya, et al. 2010), where a 12 km resolution on offshore waters resulted in overestimation of the significant wave height when compared to the 5.5 km resolution results for the same locations.

For near shore areas the model correctly simulates the coastal processes of wave propagation and transformation such as shoaling, refraction, wave breaking and energy dissipation. The results at La Parguera during Hurricane Georges show that the SWAN model results in different significant wave heights, periods and wave directions when refraction is either taken into account or not. When refraction is not activated in the model the waves follow the wind direction, thus diminishing the effects of wave transformation that occur when waves enter the coastal zone. These diminished effects are evident in the differences in significant wave heights between the refraction and no refraction cases. In the refraction case the wave heights are stabilized by refraction effects, when the waves are steered perpendicular to the coast thus increasing the energy dissipation and limiting wave growth. This limited wave growth is not seen when refraction is not active in the model, with wave height increasing proportionally to the wind forcing.

5.3 Water Level

For all simulated cases the storm surge was overestimated. This is a direct consequence of the winds being overestimated, mainly because of the lack of a land roughness length parameterization based on the land cover of each location. Qualitatively, the shape and profile of the surge follow the observations, which indicate that the Holland parametric model provides a reasonable wind profile to

force both the circulation and wave models. But to accurately reproduce the storm surge the physical processes of winds, waves, currents and water level need to be finely studied in order to be properly represented in the model for our region.

Although the wind fields are overestimated, the effect of the wind drag coefficient parameterization has to be taken in consideration as a possible contributor of error in the storm surge computation. The sensitivity of both wind and wave setup to the wind drag parameterization has been previously found in other studies . The coupled model tries to reproduce the wind-wave-circulation interactions, but still uses different wind drag parameterizations for the ADCIRC, SWAN, and unSWAN models. Moreover, there is no feedback between the models in terms of the wave growth affecting the wind drag coefficient that ADCIRC uses in the next coupling interval. The effect of the wind drag parameterization on the storm surge modeling is most evident as mesh resolution increases and near the coastal areas (Moon, Kwon, et al. 2009), the same areas where wave transformation occurs. Thus the lack of feedback between the waves and the wind forcing can negatively influence the storm surge in areas where the wind setup is the dominant mechanism, such as La Parguera, as the modeled wind is not being affected by the wave transformation processes.

Additional to the effects that the wind forcing can have on the storm surge through its momentum transfer by means of the wind stress, the timing of the storm surge is further affected by the lack of a directional land roughness parameterization in the mesh. A directional roughness length parameterization would provide a variable roughness length value (z0) that varies with the predominant wind direction at a given node (Westerink, et al. 2008). With this kind of roughness length formulation the wind forcing would increase or decrease depending on the wind direction, as well as locally changing the shape of the wind field. These changes in the local wind field would then add small-scale fluctuations in wind speed and direction that would either advance or delay in time

the modeled storm surge peak since wind speeds would be lower than they are currently in the model with no roughness length parameterization.

The results show that whether the main contributor to the storm surge is either wind or wave setup is dependent on the particular location of interest. In San Juan the main contributor was the wave setup, while in La Parguera the storm surge was driven by wind setup. This indicates that the dominant setup is determined by the particular bathymetry of the area. In San Juan there are not as many obstructions as in La Parguera, so offshore wave energy dissipation is proportionally less and wave setup becomes important in terms of its contribution to the maximum surge elevation in the near shore, where tide gauges are located. But although in La Parguera the energy dissipation caused by the bathymetry causes the wave setup to be minimal in comparison to San Juan, the residual surface elevation shows that a correct wave model configuration is necessary to appropriately the reproduce the physics in the area. For this purpose the mesh resolution clearly becomes important.

By increasing the mesh resolution in the SWAN model used for the ADCIRC+SWAN simulation not only did the wave setup diminished as a result of the energy dissipation caused by the more detailed and realistic mesh, but a bump in the water level near the end of the record was properly modeled. As this bump was not modeled neither by ADCIRC only forced by winds nor by ADCIRC+unSWAN, there is an indication that this bump is due entirely to wave forces that are properly represented with a high resolution grid. This means that by increasing the mesh resolution for the wave model not only did the surface elevation had a better agreement with the observations, but the representation of the hydrodynamics improved significantly, as no other simulation replicated this bump.

6 Conclusions

The unstructured circulation-wave model ADCIRC+SWAN was implemented for the Puerto Rico region. This model allows for the benefit of using just one computational mesh to run both the ADCIRC and SWAN models, and couple them by means of the gradient of radiation stress without the need for interpolation and with the advantage that an unstructured mesh provides of not being forced to use an structured high resolution mesh for a whole sub domain of interest, thus decreasing the computational demands.

Two different B-parameter formulations were examined to determine which provided a better wind forcing when using the Holland (1980) parametric wind model. The results show that the formulation by Holland (2008) results in the more accurate storm surge surface elevations. Wind fields were overestimated by the Holland (1980) model, but this is an effect of not using a land roughness length parameterization in the model. This was clearly seen when the observed winds were adjusted to a marine exposure land roughness, which are the conditions for which the parametric wind model was originally designed. After this adjustment the parametric and observed winds are both in the same range of magnitude, indicating that if we were to assume marine exposure at all locations the parametric winds are a good approximation to what was observed.

The results from the unstructured SWAN model were overestimated at the offshore buoy but gave reasonable results at the coastal buoy. The most notable difference for these buoys is the spatial resolution of their locations in the unstructured mesh. A resolution of about 60 km for the offshore buoy is well over the 5 km used in other studies for similar locations, while the 200 meter resolution for the coastal buoy is in the range of previous studies. The overestimation of the significant wave height on both cases is related to the overestimation of the winds by the parametric wind model, which is the primary forcing for the SWAN wave model, and the lack of wave boundary conditions

contribute to the model not being able to reproduce any swell generated outside of the principal hurricane winds area in the computational domain.

Storm surge levels were in good agreement with the observations. The overestimation of the winds by the parametric wind models caused an overestimation of the surge levels, but the maximum surges calculated by the model were in the near range of the observations. Fine-scale phenomena that determine the shape and duration of the surge, such as land roughness, has to be included in the model in order to more accurately resolve the surge. Additionally, it was shown that the contribution of either wind or wave setup as the main contributor to the surge depends on the local bathymetry of the location, and this has implications for the refinement of the mesh based on what processes dominate in a specific area. The comparison with the ADCIRC+SWAN, where SWAN had a spatial resolution of 30 meters, indicates that in order to appropriately simulate the wave processes on complex bathymetries these must be finely resolved in the model, and so an optimized refinement of the mesh must be preceded by an examination of the local contribution of waves in the area of interest, so as to avoid over solving, and increasing computational demands, in areas where wave processes are not determinant for the local hydrodynamics.

7 Works Cited

Amante, C., and B.W. Eakins. *ETOPO1 1 Arc-Minute Global Relief Model: Procedures, Data Sources and Analysis.* NOAA Technical Memorandum NESDIS NGDC-24, 2009.

Brown, Jennifer M, and Judith Wolf. "Coupled wave and surge modelling for the eastern Irish Sea and implications for model wind-stress." *Continental Shelf Research*, 2009: 1329-1342.

Bunya, S, J.C. Dietrich, J.J. Westerink, H.J. Westerink, B.A Ebersole, J.M. Smith, R. Jensen, D.T. Resio, J.H. Atkinson, H.J. Roberts, R.A. Luettich, C. Dawson, V.J. Cardone, A.T. Cox, J.D. Powell. "A High-Resolution Coupled Riverine Flow, Tide, Wind, Wind Wave, and Storm Surge Model for Southern Louisiana and Mississippi. Part I: Model Development and Validation." *Monthly Weather Review*, 2010: 345-377.

Cavaleri, L., and P. Malanotte-Rizzoli. "Wind wave prediction in shallow water: Theory and applications." *Journal of Geophysical Research*, 1981: 961-973.

Dietrich, J.C., S. Bunya, J.J. Westerink, H.J. Westerink, B.A. Ebersole, J.M. Smith, R. Jensen, D.T. Resio, J.H. Atkinson, H.J. Roberts, R.A. Luettich, C. Dawson, V.J. Cardone, A.T. Cox, J.D. Powell. "A High-Resolution Coupled Riverine Flow, Tide, Wind, Wind Wave, and Storm Surge Model for Southern Louisiana and Mississippi. Part II: Synoptic Description and Analysis of Hurricanes Katrina and Rita." *Monthly Weather Review*, 2010: 378-404.

Dietrich, J.C., M. Zijlema, J.J. Westerink, L.H. Holthuijsen, C. Dawson, R.A. Luettich Jr., R.E. Jensen, J.M. Smith, G.S. Stelling, G.W. Stone. "Modeling hurricane waves and storm surge using integrally-coupled, scalable computations." *Coastal Engineering*, 2010. In Press.

Egbert, G D, A F Bennett, and M G G Foreman. "TOPEX/POSEIDON tides estimated using a global inverse model." *Journal of Geophysical Research*, 1994: 821-24,852.

Funakoshi, Yuji, Scott Hagen, and Peter Bacopoulos. "Coupling of hydrodynamic and wave models: case study for Hurricane Floyd (1999) Hindcast." *Journal of Waterway, Port, Coastal, and Ocean Engineering*, 2008: 321-334.

Garratt, J.R. "Review of drag coefficients over oceans and continents." *Monthly Weather Review*, 1977: 915-929.

Holland, Greg. "A Revised Hurricane Pressure-Wind Model." *Monthly Weather Review*, September 2008: 3432-3445.

Hollland, Greg. "An Analytic Model of the Wind and Pressure Profiles in Hurricanes." *Monthly Weather Review*, 1980: 1212-1218.

Holthuijsen, Leo H. *Waves in Oceanic and Coastal Waters.* Cambridge: Cambridge University Press, 2007.

Komen, G.J., S. Hasselmann, and K. Hasselmann. "On the existence of a fully developed wind-sea spectrum." *Journal of Physical Oceanography*, 1984: 1271-1285.

Landsea, C. *Re-Analysys Project.* 2010. http://www.aoml.noaa.gov/hrd/data_sub/re_anal.html.
Longuet-Higgins, M.S., and R.W. Stewart. "Radiation stresses in water waves: physical discussions, with applications." *Deep Sea Research*, 1964: 529-562.

Lynch, D.R., and W.G. Gray. "A wave equation model for finite element tidal computations." *Computational Fluids*, 1979: 207-228.

Mastenbroek, C, G Burgers, and A.E.M. Janssen. "The dynamical coupling of a wave model and a storm surge model through the atmospheric boundary layer ." *Journal of Physical Oceanography*, 1992: 1856-1866.

Moon, Il-Ju, Jae-Il Kwon, Jong-Chan Lee, Jae-Sol Shim, Sok Kuh Kang, Im Sang Oh,Seok Jae Kwon. "Effect of the surface wind stress parameterization on the storm surge modeling." *Ocean Modelling*, 2009: 115-127.

Moon, Il-Ju, Isaac Ginis, and Tetsu Hara. "Effect of Surface Waves on Air-Sea Momentum Exchange. Part II: Behavior of Drag Coefficient Under Tropical Cyclones.=." *Journal of the Atmospheric Sciences*, 2004: 2334-2348.

Moon, Il-Ju, Isaac Ginis, Tetsu Hara, Hendrick L Tolman, C.W. Wright, and Edward J Walsh. "Numerical Simulation of Sea Surface Directional Wave Spectra under Hurricane Wind Forcing." *Journal of Physical Oceanography*, 2003: 1680-1706.

Moon, Il-Ju, Tatsu Hara, and Isaac Ginis. "Effect of Surface Waves on Air-Sea Momentum Exchange. Part I: Effect of Mature and Growing Seas." *Journal of the Atmospheric Sciences*, 2004: 2321-2333.

Morelock, J. "Shoreline of Puerto Rico." Coastal Zone Management Program, Department of Natural Resources, Puerto Rico, 1978.

National Geophysical Data Center. *NOAA Tsunami Inundation Digital Elevation Models (DEMs) for the Caribbean Region.* 2010. http://www.ngdc.noaa.gov/dem/selectdem.jsp?regionName=Caribbean (accessed 07 2010).

Peng, Machuan, Lian Xie, and Leonard J Pietrafesa. "Tropical cyclone induced assymetry of sea level surge and fall and its presentation in a storm surge model with parametric wind fields." *Ocean Modelling*, 2006: 81-101.

Phadke, Amal C, Christopher D Martino, Kwok Fai Cheung, and Samuel H Houston. "Modeling of tropical cyclone winds and waves for emergency management." *Ocean Engineering*, 2003: 553-578.

Powell, Mark D, and Samuel H Houston. "Hurricane Andrew's Landfall in South Florida. Part I: Standardizing Measurements for Documentation of Surface Wind Fields." *Weather and Forecasting*, 1996: 304-328.

Steyaerd, Louis T, and Robert G Knox. "Reconstructed historical land cover and biophysical parameters for studies of land-atmosphere interactions within the easter United States." *Journal of Geophysical Research*, 2008.

Westerink, J.J., R.A. Luettich, A.M. Baptista, N.W. Scheffner, and P. Farrar. "Tide and storm surge predictions using finite element model." *Journal of Hydraulic Engineering*, 1992: 1373-1390.

Westerink, Joannes J.,.R. Luettich A, J.C. Feyen, J.H. Atkinson, C. Dawson, H.J. Roberts, M.D. Powell, J.P. Dunion, E.D. Kubatko, H. Pourtaheri. "A Basin- to Channel-Scale Unstructured Grid Hurricane Storm Surge Model Applied to Southern Louisiana." *Monthly Weather Review*, 2008: 833-864.

Willmott, Court J. "Some Comments on the Evaluation of Model Performance." *Bulletin American Meteorological Society*, 1982: 1309-1313.

Wu, J. "Wind-stress coefficients over a sea surface from breeze to hurricane." *Journal of Geophysical Research*, 1982: 9704-9706.

Xie, Lian, Huiqing Liu, and Machuan Peng. "The effect of wave-current interactions on the storm surge and inundation in Charlestone Harbor during Hurricane Hugo 1989." *Ocean Modelling*, 2008: 252-269.

Xie, Lian, Shaowu Bao, Leonard J Pietrafesa, Kristen Foley, and Montserrat Fuentes. "A Real-Time Hurricane Surface Wind Forecasting Model: Formulation and Verification." *Monthly Weather Review*, 2006: 1355-1370.

Young, I R. "A review of the sea state generated by hurricanes." *Marine Structures*, 2003: 201-218.

Young, Ian R. *Wind Generated Ocean Waves.* Oxford: Elsevier, 1999.

Zijlema, M. "Computation of wind-wave spectra in coastal waters with SWAN on unstructured grids." *Coastal Engineering*, 2010: 267-277.